Journal of Wind Engineering & Industrial Aerodynamics 211 (2021) 104527

Contents lists available at ScienceDirect

Journal of Wind Engineering & Industrial Aerodynamics

journal homepage: www.elsevier.com/locate/jweia

Large-eddy simulation of pollutant dispersion in generic urban street canyons: Guidelines for domain size

Xing Zheng [a,*], Hamid Montazeri [a], Bert Blocken [a,b]

[a] Building Physics and Services, Department of the Built Environment, Eindhoven University of Technology, P.O. Box 513, 5600 MB, Eindhoven, the Netherlands
[b] Building Physics & Sustainable Design, Department of Civil Engineering, KU Leuven, Kasteelpark Arenberg 40 - Bus 2447, 3001, Leuven, Belgium

ARTICLE INFO

Keywords:
Computational fluid dynamics
Air quality
Urban ventilation
LES simulation
Best practice guidelines
Pollutant removal
Built environment
Air pollution
Urban wind flow
Contaminant dispersion

ABSTRACT

Pollutant dispersion in urban street canyons has been widely investigated by large-eddy simulation (LES). Many LES studies focused on generic street canyons under a wind direction perpendicular to the street axis. Accurate LES simulations require a sufficiently large domain size to minimize the effects of the artificial boundary conditions at the domain faces on the results. As opposed to RANS simulations, there is a lack of guidelines for an appropriate domain size for LES simulations of wind flow and pollutant dispersion in street canyons. The present study systematically investigates the effect of the domain width, domain height and upstream and downstream domain lengths on the wind flow and pollutant dispersion within a generic 2.5D street canyon with spanwise periodic boundary conditions. Following a validation study, 16 LES simulations are performed for different domain sizes. The results show that the minimum requirement for the domain width is 2.5H, where H is the roof height of the street canyon. For the domain height, upstream domain length and downstream domain length, 7.5H, 5H and 10H are recommended, respectively. These guidelines should help to reduce the computational costs of this type of simulation without significantly compromising the accuracy.

1. Introduction

Air pollution is a world-wide problem. The World Health Organization (WHO) reported in 2016 that more than 80% of people living in urban areas are exposed to levels of air pollution higher than the limits recommended for health reasons (World Health Organization, 2016). For a better prediction and understanding of the air quality and pollutant dispersion in the urban canopy, knowledge about the interactions between urban-canopy elements and the atmosphere is important (Kastner-Klein and Plate, 1999; Vervoort et al., 2019). Urban street canyons are basic urban-canopy elements where long narrow streets are bordered by building walls on both sides. They are known to be susceptible to high air pollution concentrations, certainly when the wind direction is perpendicular to the street axis (Kastner-Klein et al., 2004; Oke, 1988). Flow and dispersion fields inside and in the vicinity of urban street canyons are important aspects of urban air-quality studies (Antoniou et al., 2019; Baik et al., 2012; Ricci et al., 2019; Scungio et al., 2018). Apart from wind/water tunnel testing (Baratian-Ghorghi and Kaye, 2013; Gromke and Ruck, 2007, 2009; Kastner-Klein and Plate, 1999; Li et al., 2008a; Meroney et al., 1996; Nosek et al., 2017; Stabile et al., 2015), computational fluid dynamics (CFD) has been used to investigate pollutant dispersion in street canyons under the perpendicular wind. Many CFD studies have adopted the Reynolds-averaged Navier–Stokes (RANS) approach (Ding et al., 2019; He et al., 2017; Huang et al., 2016; Mei et al., 2016; Vranckx et al., 2015; Wen and Malki-Epshtein, 2018; Xie et al., 2020; Zhang et al., 2019). In the past decades, an increasing number of studies have been performed with large-eddy simulation (LES) (Antoniou et al., 2017; Blocken, 2018; Lateb et al., 2016; Salim et al., 2011a; Tominaga and Stathopoulos, 2011). LES resolves the large-scale unsteady motions and allows the reproduction of the highly transient nature of wind velocity and pollutant concentration in street canyons (Tominaga and Stathopoulos, 2013), which can lead to strongly improved accuracy (Tominaga and Stathopoulos, 2011).

Even though LES is intrinsically superior over RANS, LES results tend to be more sensitive to the many computational settings and parameters that have to be set by the user (Blocken, 2018), including the size of the computational domain, the computational grid topology, and the boundary conditions. A non-exhaustive overview of LES studies on generic street canyons under a perpendicular wind is provided in Table 1. These generic street canyons are categorized into type A (Fig. 1a), where the buildings are represented by protrusions above the bottom of the domain, and type B, where the canyon cavity is represented by a

* Corresponding author.
E-mail address: x.zheng.1@tue.nl (X. Zheng).

https://doi.org/10.1016/j.jweia.2021.104527
Received 11 October 2020; Received in revised form 31 December 2020; Accepted 10 January 2021
Available online 5 March 2021
0167-6105/© 2021 The Authors. Published by Elsevier Ltd. This is an open access article under the CC BY license (http://creativecommons.org/licenses/by/4.0/).

Table 1
Overview of studies on wind flow and associated processes in generic street canyons using LES.

Ref.	Type	Aspect ratio (= H/W)	2.5D (if yes, domain width (W_d))	Spanwise boundary conditions	Domain height (H_d)	Scale
Walton and Cheng (2002)	B	1.2	Yes (1.25H)	Periodic	3.1H	Full
Liu et al. (2004)	B	0.5, 1.0, 2.0	Yes (1H)[a]	Periodic	–	Reduced
Baker et al. (2004)	B	1	Yes (2.2H)	Periodic	5.2H	Full
Li et al. (2008b)	B	1.0, 2.0, 3.0, 5.0	Yes (–)	Periodic	2H[a]	Reduced
Hu et al. (2009)	B	1	Yes (2.2H)	–	2.2H	Full
Li et al. (2010)	B	1	Yes (–)	Periodic	2H	Reduced
Salim et al. (2011a)	A	1	No	Symmetry	8H	Reduced
Salim et al. (2011b)	A	1	No	Symmetry	8H	Reduced
Moonen et al. (2011)	B	1	No	Periodic	9H	Full
Zhang et al. (2011)	B	1	Yes (2H)	Periodic	2H	Full
Cheng and Liu (2011)	B	1	Yes (5H)	Periodic	6H	–
Park et al. (2012)	B	1	Yes (2H)	Periodic	5.5H	Full
Kikumoto and Ooka (2012a)	A	1	Yes (3H)	Periodic	8H	Full
Kikumoto and Ooka (2012b)	A	1.0, 2.0	Yes (3H)[a]	Periodic	8H[a]	Full
Moonen et al. (2013)	A	1	No	Symmetry	8.3H	Reduced
Bright et al. (2013)	B	1	Yes (1.7H)	Periodic	5.2H	Full
Lo and Ngan (2015)	B	1	Yes (2H)	Periodic	3H	Full
Zhong et al. (2015)	B	2	Yes (1.1H)	Periodic	3.1H	Full
O'Neill et al. (2016)	B	1	Yes (2.2H)	Periodic	5.2H	Full
Zhong et al. (2017)	B	2	Yes (1.1H)	Periodic	3.1H	Full
Llaguno-Munitxa et al. (2017)	A	1	Yes (12H)	Wall	8H	Reduced
Llaguno-Munitxa and Bou-Zeid (2018)	A	1	Yes (12H)	Wall	8H	Reduced
Merlier et al. (2018)	A	1	No	Wall	8.3H	Reduced
Wang et al. (2018)	A	0.2, 0.5, 1.0, 5.0	Yes (15H)[a]	Periodic	5H[a]	Full
Han et al. (2018)	A	1	Yes (1.5H)	Periodic	5H	Full
Duan and Ngan (2018)	B	1	Yes (1.92H)	Periodic	3H	Full
Chew et al. (2018)	B	1	Yes (1H)	Periodic	6H	Reduced
Gallagher and Lago (2019)	B	1	Yes (10H)	–	1.5H	Full
Chatzimichailidis et al. (2019)	B	1	Yes (0.5H)	Periodic	3, 4, 5, 6H	Full

– = information has not been provided, Symmetry = zero normal gradients of all variables and zero normal velocity.
[a] For the studies considering more than one aspect ratio, H is the roof height of the case with an aspect ratio of 1.

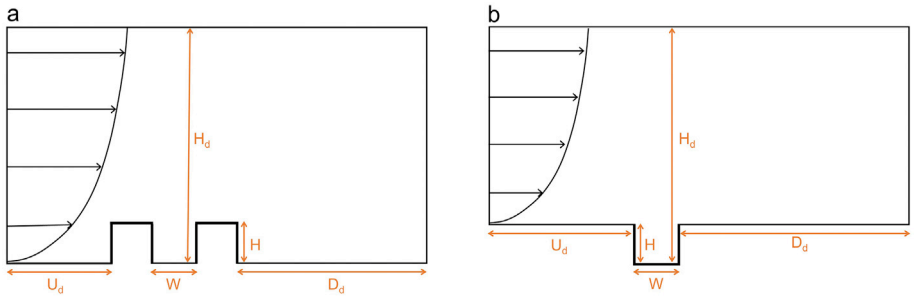

Fig. 1. (a) Configuration of street canyon type A and (b) same for type B.

recession in the bottom of the domain (Fig. 1b). Table 1 indicates that most studies focused on typical street canyons that have the aspect ratio (= building roof height H divided by street width W) equal to 1. Moreover, generic street canyons have been commonly simulated in full scale and treated as spanwise homogeneous 3D geometries, namely 2.5D (Geng et al., 2018) or quasi-2D (Chatzimichailidis et al., 2019) simulations. Periodic boundary conditions have generally been applied in the spanwise direction to reduce the size of the computational domain. From Table 1, it can be observed that a wide range of different values of domain width, ranging from H to 15H have been used for 2.5D street canyons. This is also the case for the domain height, which ranged from 5H to 8H for canyon type A and 1.5H to 6H for type B.

In CFD simulation of 2.5D street canyons, a small domain height inevitably leads to a large blockage ratio, which can artificially accelerate the airflow and affect the simulation (Franke et al., 2007; Tominaga et al., 2008). A recent study (Chatzimichailidis et al., 2019) has examined the influence of domain height for a 2.5D street canyon of type B. The mean concentrations obtained with domain heights of 3H, 4H, 5H and 6H were compared. The results showed that the smaller the height of the domain, the lower the mean concentration at the windward side. The results with H_d = 6H were found to be marginally closer to the experimental data than the other domain heights (Chatzimichailidis et al., 2019). For 2.5D street canyons, although periodic boundary conditions are used in the spanwise direction, also a sufficient domain width is necessary to ensure the resolving of the largest coherent eddies occurring within the canyon. To the best of our knowledge, a sensitivity analysis on the minimum requirement for the domain width has not yet been performed.

Several documents providing best practice guidelines – albeit mainly for RANS simulations – have been provided in the past two decades. These include requirements for the size of the computational domain and the topology of the grid (Ai and Mak, 2017; Blocken, 2015; Franke et al, 2007, 2011; Meroney et al., 2016; Ramponi and Blocken, 2012; Tominaga et al., 2008). For example, guidelines (Franke et al., 2011) suggested that the inlet, lateral and top boundaries should be at least $5H_{max}$ (where H_{max} is the height of the tallest building) away from the building group. The full blockage ratio is defined as the ratio of the projected frontal (windward) area of the obstacles to the cross-sectional area of the computational domain, which should not be larger than 3%. The guidelines by Tominaga et al. (2008) also recommended a maximum full blockage ratio of 3%. They demanded the outflow boundary to be at least $10H_{max}$ away from the building group. Blocken (2015) proposed the concept of two directional blockage ratios, one in the horizontal and one

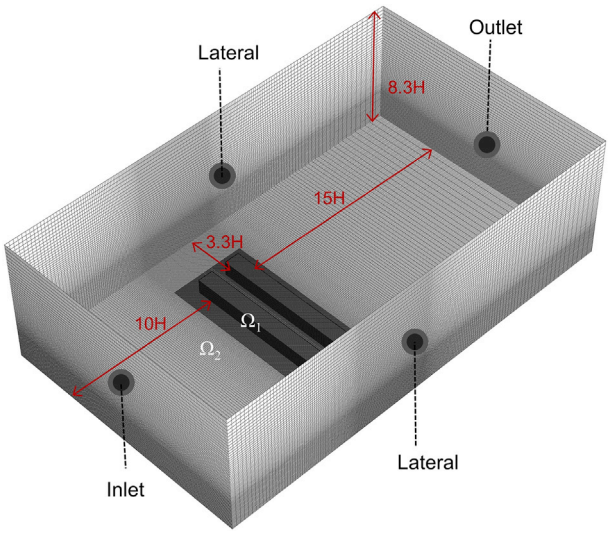

Fig. 2. Computational domain, grid, and boundary conditions of the basic grid (11.9 million cells).

in the vertical direction, which consists of the decomposition of the full blockage ratio, i.e. 17% (square root of 3%). This is to avoid unwanted artificial acceleration in some exceptional situations, e.g. for very wide buildings or for urban models with horizontal dimensions that are much larger than the vertical dimensions. However, as mentioned earlier, the vast majority of these guidelines are directed to RANS simulations. Only a few best practice guidelines for building and urban aerodynamics simulations have been developed for LES (Ai and Mak, 2015; Gousseau et al., 2013; Iousef et al., 2017; Vasaturo et al., 2018). It has been argued that this is one of the reasons why LES is not applied more frequently for such applications (Blocken, 2018). Another reason is that the establishment of guidelines has to be based on many LES simulations in extensive sensitivity studies (Blocken, 2018; Hanjalic, 2005). The present study aims to provide some guidelines on the domain size for LES. The focus will be on street canyons of type A (Fig. 1a), which is considered a more common and more realistic representation of a street canyon than type B.

The outline of the paper is as follows: Section 2 presents the CFD validation study. Section 3 introduces the reference case, the test matrix for the sensitivity study of the domain size, the boundary conditions, and the other computational settings for the LES simulations. The results of the sensitivity study on the domain width, domain height and domain lengths are presented in Sections 4, 5 and 6, respectively. Finally, discussion (Section 7) and conclusions and recommendations (Section 8) are provided.

Table 2
Characteristics of the grids for the grid-sensitivity analysis and the associated time steps.

	Grid size in Ω_1	Time step Δt	# cells (million)
Grid 1 (Coarse)	0.0040 m (H/30)	0.00025 s	5.5
Grid 2 (Basic)	0.0030 m (H/40)	0.00019 s	11.9
Grid 3 (Fine)	0.0025 m (H/48)	0.00017 s	20.4

2. Validation study

2.1. Description of the wind-tunnel experiment

In the wind-tunnel measurement by Gromke and Ruck (2009), the mean velocity field and the mean concentration of the tracer gas in a long street canyon model were measured in an open-circuit atmospheric boundary layer wind-tunnel at the Karlsruhe Institute of Technology. Note that in this experiment, different cases were considered with and without trees. In the present validation study, the results of the 1:1 aspect ratio street canyon without trees were used. The street canyon model, at the scale of 1:150, consisted of two parallel buildings of 0.12 m × 0.12 m × 1.2 m each (streamwise (x) × vertical (z) × spanwise (y) dimensions). The width of the street between the two parallel buildings was 0.12 m, yielding an aspect ratio equal to 1. The approach-flow wind was perpendicular to the street axis. The approach-flow profiles represented a turbulent boundary layer flow with power-law exponent $\alpha = 0.30$ for the mean velocity and $\alpha_I = 0.36$ for the turbulence intensity, with values of mean velocity (U_{ref}) and turbulence intensity at the roof height equal to 4.65 m/s and 16.20%, respectively (Gromke, 2008a). The streamwise pressure gradient was reduced by adjusting the wind-tunnel ceiling when the street canyon model was set up in the test section (Gromke and Ruck, 2009).

Sulfur hexafluoride (SF_6) was used as a tracer gas. The release of traffic exhausts was modeled by a tracer gas mixture that was emitted from four line sources mounted at the bottom of the model. The line source strength was controlled and monitored by a flow controller of type 1259B from MKS instruments and flow meter of type 1258B, ensuring a constant tracer gas supply during the measurements (Gromke and Ruck, 2009). To sample the near-wall canyon air, each wall facing the street was equipped with concentration measurement taps protruding 5 mm out of the wall. An electron capture detector (model: Meltron LH 108) was used to analyze the mean concentration (Buccolieri et al., 2009; Gromke et al., 2008). The mean concentration of SF_6 was expressed in dimensionless as follows:

$$C^+ = \frac{CU_{ref}H}{Q/l} \quad (1)$$

where C is the measured mean concentration, U_{ref} is the undisturbed approach-flow mean wind velocity at the building roof height H, and Q/l is the emission rate of the tracer gas per unit length. According to

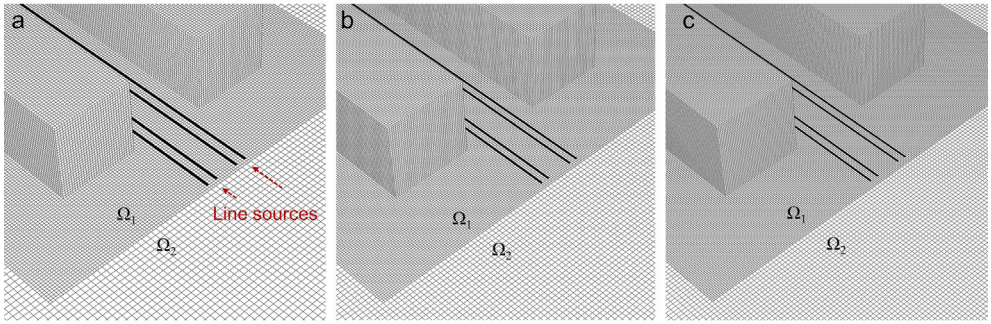

Fig. 3. LES computational grids near bottom of domain: (a) coarse grid (5.5 million cells), (b) basic grid (11.9 million cells) and (c) fine grid (20.4 million cells). The four black lines indicate the line sources.

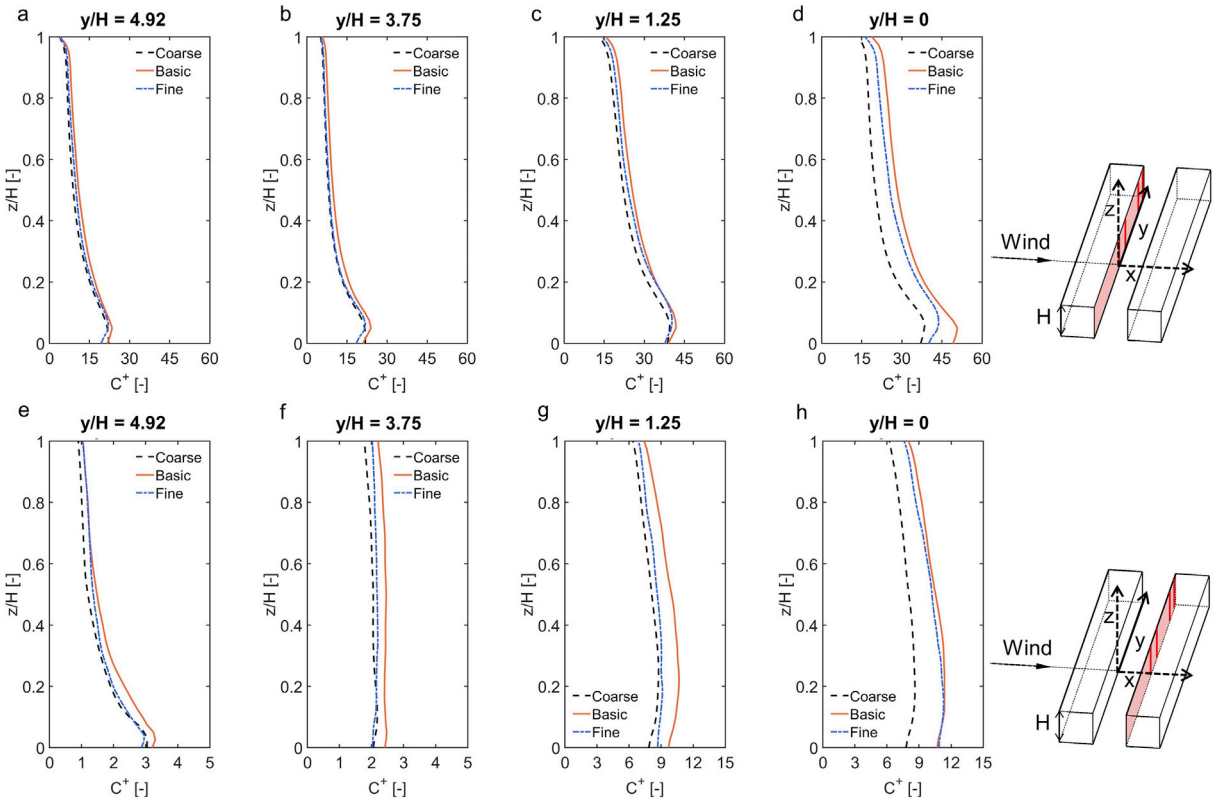

Fig. 4. Results of grid-sensitivity study along four vertical lines near (a–d) the leeward wall: (a) y/H = 4.92; (b) y/H = 3.75; (c) y/H = 1.25; (d) y/H = 0; (e–h) same near the windward wall.

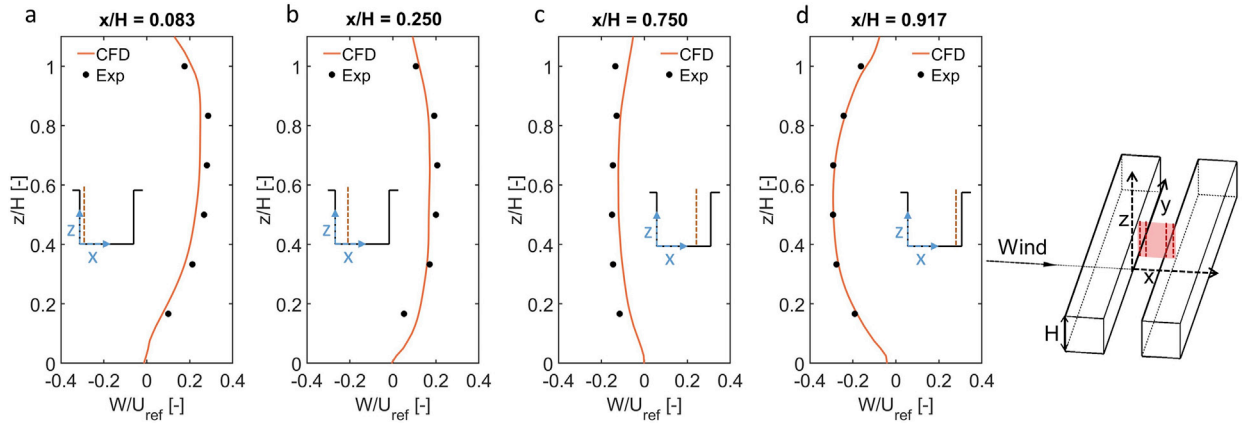

Fig. 5. Comparisons between the measured and simulated dimensionless mean vertical velocity component (W/U_{ref}) along four vertical lines in the vertical plane near the canyon center (y/H = 0.5): (a) x/H = 0.083; (b) x/H = 0.25; (c) x/H = 0.75; (d) x/H = 0.917.

Ref. (Gromke, 2008b), the uncertainty of the measurement depended on the measured mean concentration. The smaller mean concentrations led to larger percentage errors that could go up to 14.0%, while the larger mean concentrations led to lower percentage errors that less than 2.5%.

Velocity measurements were performed using Laser-doppler Velocimetry (LDV). The LDV-system incorporated a 4 Watt argon-ion laser and an optical system. The mean vertical velocity component (W) was measured in a vertical plane perpendicular to the street axis near the center of the canyon (Gromke and Ruck, 2009).

2.2. Computational domain and grid

A computational domain is made of the street canyon in the wind-tunnel. The geometry is reproduced at the wind-tunnel scale. Fig. 2 illustrates the computational domain and grid. The width and height of the computational domain are equal to the width and height of the wind-tunnel, i.e. 2 m and 1 m, respectively. The upstream and downstream domain lengths are 1.2 m (10H) and 1.8 m (15H), respectively.

A non-conformal grid is generated. The entire domain is divided into two subdomains, an inner domain Ω_1 and an outer domain Ω_2. Subdomain Ω_1 is extended up to a distance of 1H away from the model (see Fig. 2). Cubic cells with an edge length of 0.003 m (H/40) are applied in subdomain Ω_1. As recommended in Ref. (Iousef et al., 2017), a grid refinement ratio of 1:2 is applied between the adjacent subdomains. Subdomain Ω_2 is discretized with hexahedral cells with a stretching ratio of 1.05. The total number of cells is 11.9 million. The grid resolution is

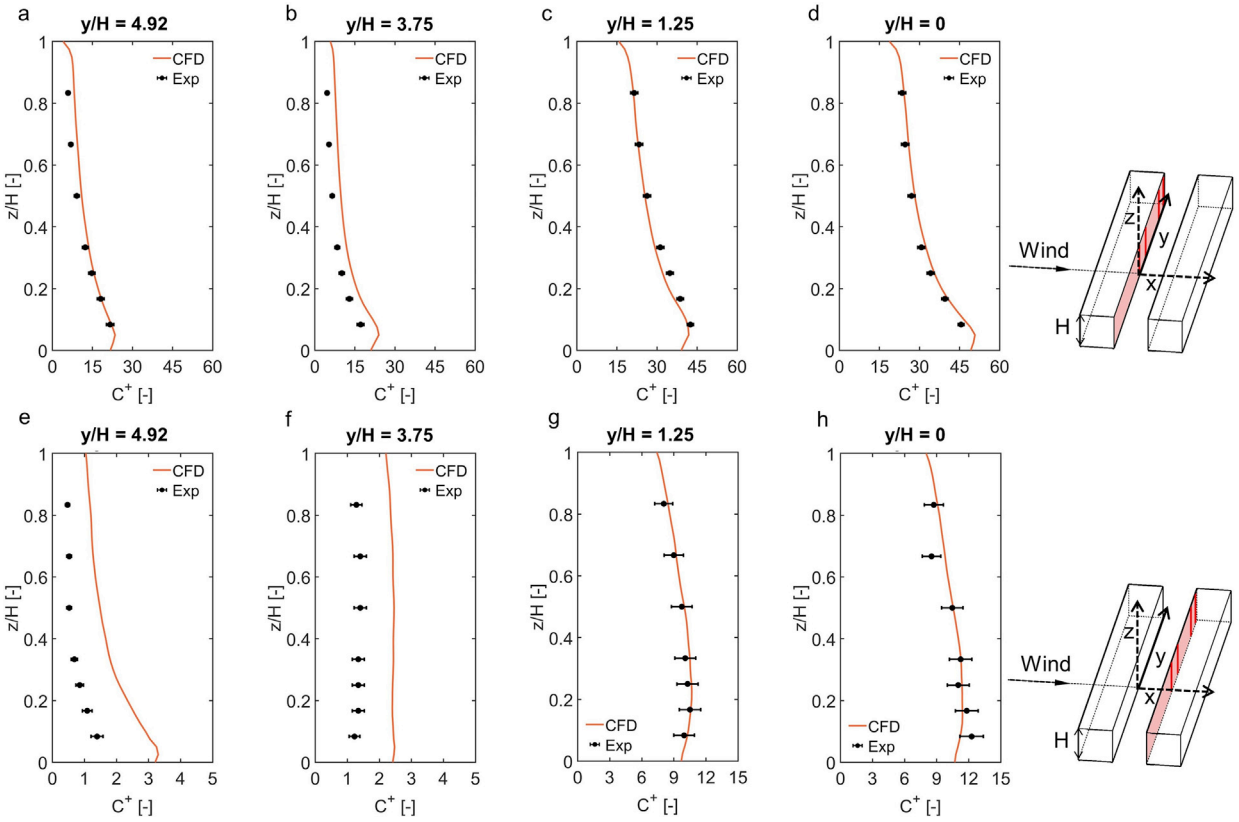

Fig. 6. Comparisons between the measured and simulated C^+ along four vertical lines near the leeward wall: (a) y/H = 4.92; (b) y/H = 3.75; (c) y/H = 1.25; (d) y/H = 0; (e-h) same for the windward wall. The error bar is added according to the measurement uncertainty reported in Ref. (Gromke, 2008b).

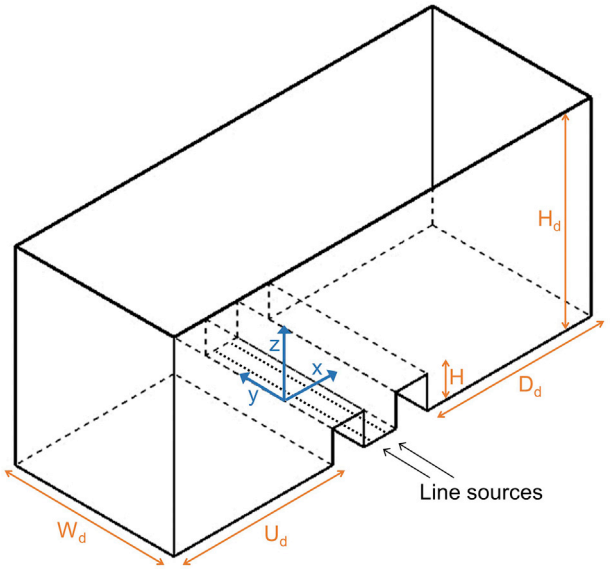

Fig. 7. Schematic of the computational domain: W_d, domain width; U_d, upstream domain length; D_d, downstream domain length; and H_d, domain height.

based on a grid-sensitivity analysis. Further information about the grid-sensitivity analysis will be provided in Subsection 2.4.

2.3. Boundary conditions and solver settings

No-slip walls are used for the top, bottom and lateral boundary conditions to reproduce the test section ceiling, ground and side walls in the experiment, respectively. No-slip walls are also applied on the surfaces of the canyon model. All walls are considered impermeable for species transport. For the inlet boundary conditions, the measured profiles of mean wind speed and turbulent kinetic energy (Gromke, 2008a) are used. The turbulence dissipation rate ε is calculated using Eq. (2) (Richards and Hoxey, 1993).

$$\varepsilon(z) = \frac{u^{*3}_{ABL}}{\kappa(z + z_0)} \tag{2}$$

where the friction velocity $u^*_{ABL} = 0.59$ m/s and the roughness length $z_0 = 0.004$ m (wind-tunnel scale, obtained from logarithmic law curve fitting of the mean velocity profile in the wind-tunnel (Gromke, 2008a)). The von Karman constant κ is 0.42. Time-dependent inlet conditions are generated by the vortex method (Mathey et al., 2006; Sergent, 2002). The number of vortices N_V takes 6700, which is estimated by $N_V = N/4$ (where N = number of inlet grid cells) (Gerasimov, 2016). Four line sources with 1.42 m × 0.003 m (reduced-scale values) are created on the domain bottom boundary (Fig. 3). According to the wind-tunnel experiment (Gromke, 2008a), the lines are located at about 0.23H, 0.35H, 0.65H and 0.77H from the leeward wall. The exhaust faces are velocity inlets injecting pure SF_6 in the domain with a constant velocity of 0.096 m/s. This results in an emission rate of Q = 10 g/s (Gromke et al., 2008).

The commercial CFD code ANSYS Fluent 18.0 is employed (ANSYS Inc, 2017). The LES simulation is started from the solution of a 3D steady RANS simulation. For the steady RANS simulation, the realizable k-ε turbulence model is used with turbulent Schmidt number of 0.7 (Tominaga and Stathopoulos, 2007). For pressure-velocity coupling, the SIMPLE algorithm is used. Pressure interpolation is second order and second-order discretization schemes are applied for both the convection and viscous terms of the governing equations.

Table 3
Test matrix for the sensitivity analysis. All sizes are given in the roof height of the street canyon (H). Note that for clarity the reference domain (marked as *) is listed four times (once for each parameter).

Parameter	W_d	H_d	Blockage ratio	U_d	D_d	# cells (million)
Domain width (W_d)	1.25	11.0	9.1%	10	10	0.97
	2.00					1.55
	2.50					1.94
	3.75					2.91
	5.00*					3.89
	7.50					5.82
Domain height (H_d)	5.00	3.0	33.3%			3.28
		5.0	20.0%			3.51
		6.0	16.7%			3.59
		7.5	13.3%			3.71
		11.0*	9.1%			3.89
		21.0	4.7%			4.16
Upstream domain length (U_d)	5.00	11.0	9.1%	10*	10	3.89
				7.5		3.77
				5		3.63
				2.5		3.61
Downstream domain length (D_d)	5.00	11.0	9.1%	10	10*	3.89
					6	3.63
					3	3.61

LES simulations are conducted with the wall-adapting local eddy viscosity model (WALE) (Ducros et al., 1998) with the constant C_{wale} = 0.325. Pressure-velocity coupling is performed using the fractional step method in combination with the non-iterative time advancement (NITA) scheme. For pressure interpolation and time discretization, second-order schemes are applied. A second-order upwind scheme is used for the energy and SF_6 concentration equations. Werner-Wengle wall functions that assume either a linear or 1/7 power-law distribution of instantaneous velocity in the first cell, are applied (ANSYS Inc, 2017; Werner and Wengle, 1993). The time step (Δt) is 0.00019 s, and the resulting maximum and volume-averaged Courant-Friedrichs-Lewy (CFL) numbers are 0.98 and 0.11, respectively. Before the start of data averaging, the LES simulation runs during 7.3 s, corresponding to approximately 10 flow-through times ($T_{flow\text{-}through} = L_x/U_{ref}$, where L_x is the length of the computational domain and U_{ref} = 4.65 m/s). After this LES initialization step, data are averaged over a period of 25 s (approximately 35 flow-through times) (Salim et al., 2011a, 2011b).

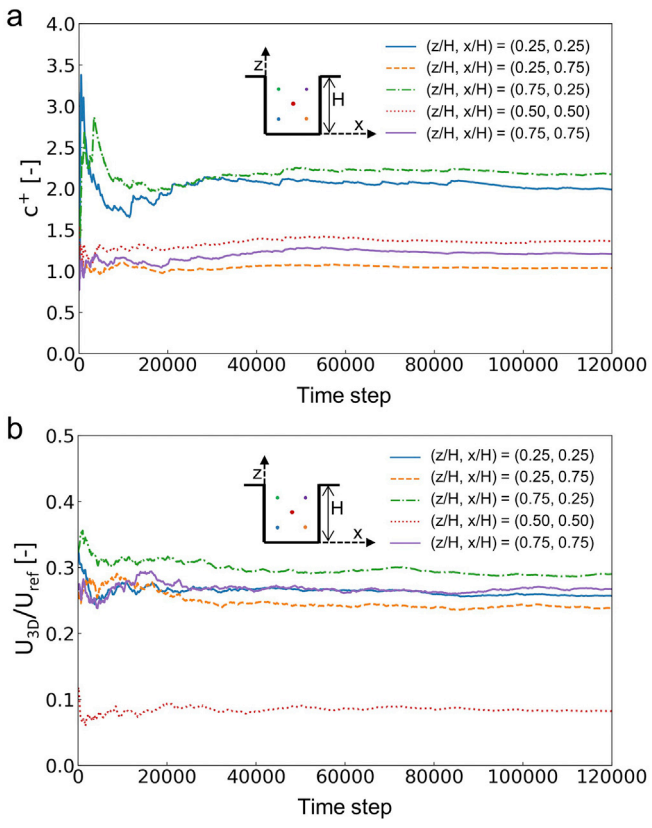

Fig. 8. Convergence monitoring for the reference case: (a) C^+ and (b) U_{3D}/U_{ref} at five points as a function of time step.

2.4. Grid-sensitivity study

In order to assess the grid dependence, a fine, basic and coarse grid are made based on the same overall grid topology. Table 2 describes the characteristics of the three grids. The fine and coarse grid have 20.4 million and 5.5 million cells, respectively. For subdomain Ω_1, the edge lengths of the cubic cells are H/48 and H/30 for the fine and coarse grid, respectively (Fig. 3). The time steps of 0.00017 s and 0.00025 s are set for the fine and coarse grid, respectively, to ensure the maximum Courant-Friedrichs-Lewy number lower than 1.

Fig. 4a–d compares the profiles of C^+ obtained by the three grids along four vertical lines near the leeward wall: y/H = 4.92, 3.75, 1.25 and 0, respectively. The profiles along four vertical lines near the windward wall: y/H = 4.92, 3.75, 1.25 and 0 are compared in Fig. 4e–h, respectively. Note that the lines are 5 mm away from the walls. Significant differences between the results obtained by the coarse grid and basic grid are observed. The average percentage differences between the results obtained by the coarse grid and basic grid are 16.40% and 16.01% for the lines near the leeward wall and windward wall, respectively. Less differences are found between the results obtained by the fine grid and the basic grid. In this case, the average percentage differences are 8.62% and 5.40%, for the lines near the leeward wall and windward wall, respectively. It is, therefore, concluded that the basic grid can be retained for the validation study.

2.5. Results

The CFD results are compared with the wind-tunnel data in terms of the dimensionless mean vertical velocity component (W/U_{ref}) and C^+ (Gromke and Ruck, 2007, 2009).

Fig. 5 shows a comparison between the simulated and measured W/U_{ref} along four vertical lines in the vertical plane near the canyon center (y/H = 0.5): x/H = 0.083, 0.250, 0.750 and 0.917. The agreement between CFD and measurements is good, especially for the points with relatively high wind speeds. The average absolute differences of W/U_{ref} along the four lines are 0.03, 0.03, 0.04 and 0.01, respectively.

Fig. 6 depicts the comparison between the simulated and measured

Table 4
Convergence monitoring: e_{conv} (%) of C^+ and U_{3D}/U_{ref} at the five points in the vertical centerplane (y/H = 0) for 12 equidistant intervals in the averaging period.

		(z/H, x/H) = (0.25, 0.25)		(z/H, x/H) = (0.25, 0.75)		(z/H, x/H) = (0.75, 0.25)		(z/H, x/H) = (0.5, 0.5)		(z/H, x/H) = (0.75, 0.75)	
I	Range of time step	e_{conv} (C^+)	e_{conv} (U_{3D}/U_{ref})	e_{conv} (C^+)	e_{conv} (U_{3D}/U_{ref})	e_{conv} (C^+)	e_{conv} (U_{3D}/U_{ref})	e_{conv} (C^+)	e_{conv} (U_{3D}/U_{ref})	e_{conv} (C^+)	e_{conv} (U_{3D}/U_{ref})
1	1–10000	141.62	29.57	23.92	15.93	79.46	17.50	36.80	74.36	36.86	16.49
2	10001–20000	15.18	6.63	12.62	9.31	6.42	3.83	6.24	22.56	11.33	11.25
3	20001–30000	9.77	3.68	3.44	6.42	7.01	3.90	4.99	8.65	7.69	6.00
4	30001–40000	2.39	2.26	4.52	3.13	2.88	3.80	5.08	9.24	6.80	3.38
5	40001–50000	3.84	1.69	1.49	2.80	4.18	1.89	2.48	10.16	4.12	3.05
6	50001–60000	2.36	1.34	1.89	1.11	2.29	1.43	1.66	8.61	2.20	3.64
7	60001–70000	2.01	1.16	2.07	2.33	1.48	1.84	2.93	5.32	2.48	2.81
8	70001–80000	1.44	2.57	1.33	2.05	0.95	2.59	1.16	5.54	1.89	1.84
9	80001–90000	2.61	1.55	0.71	1.97	1.39	1.39	1.61	4.06	1.30	1.41
10	90001–100000	3.20	1.34	1.15	2.71	1.88	1.04	1.03	3.08	1.53	2.46
11	100001–110000	0.95	0.97	0.60	1.88	0.79	0.92	1.81	2.05	1.28	1.93
12	110001–120000	1.17	0.43	0.41	1.27	1.14	1.38	0.84	1.73	0.97	1.37

C^+ along vertical lines: y/H = 4.92, 3.75, 1.25 and 0 near the leeward and windward walls. For the four lines near the leeward wall, the average absolute differences of C^+ are 1.38, 3.37, 1.50 and 1.46, respectively (Fig. 6a–d). For the windward wall, the average absolute differences along lines y/H = 4.92 and 3.75 are 1.07 and 1.01, respectively (Fig. 6e and f). The possible reason of these relatively large differences is the underestimation of wind speed near the corner of the canyon. For the other two lines closer to the center of the canyon, y/H = 1.25 and 0, good agreements are observed with average absolute differences of 0.14 and 0.53, respectively (Fig. 6g and h). This validation study shows that the LES simulation in combination with high-resolution grids, Werner-Wengle wall functions, and other solver settings can provide a satisfactory agreement of the mean wind velocity and mean concentration for a long street canyon, especially near the center of the canyon. Therefore, LES with the same grid resolution, sub-grid scale model, wall functions, and solver settings will be used for the sensitivity analysis with a focus on the center region of the canyon.

3. Sensitivity analysis: reference case

3.1. Computational domain and grid

A reference case is defined as a starting point for the domain size sensitivity analysis. The simulations are performed at full scale. The 2.5D street canyon has a building height of 12 m and a street width of 12 m. A computational domain is made of the generic street canyon of type A (Fig. 7). It includes an initial domain width (W_d) of 5H, domain height (H_d) of 11H, upstream domain length (U_d) of 10H and downstream

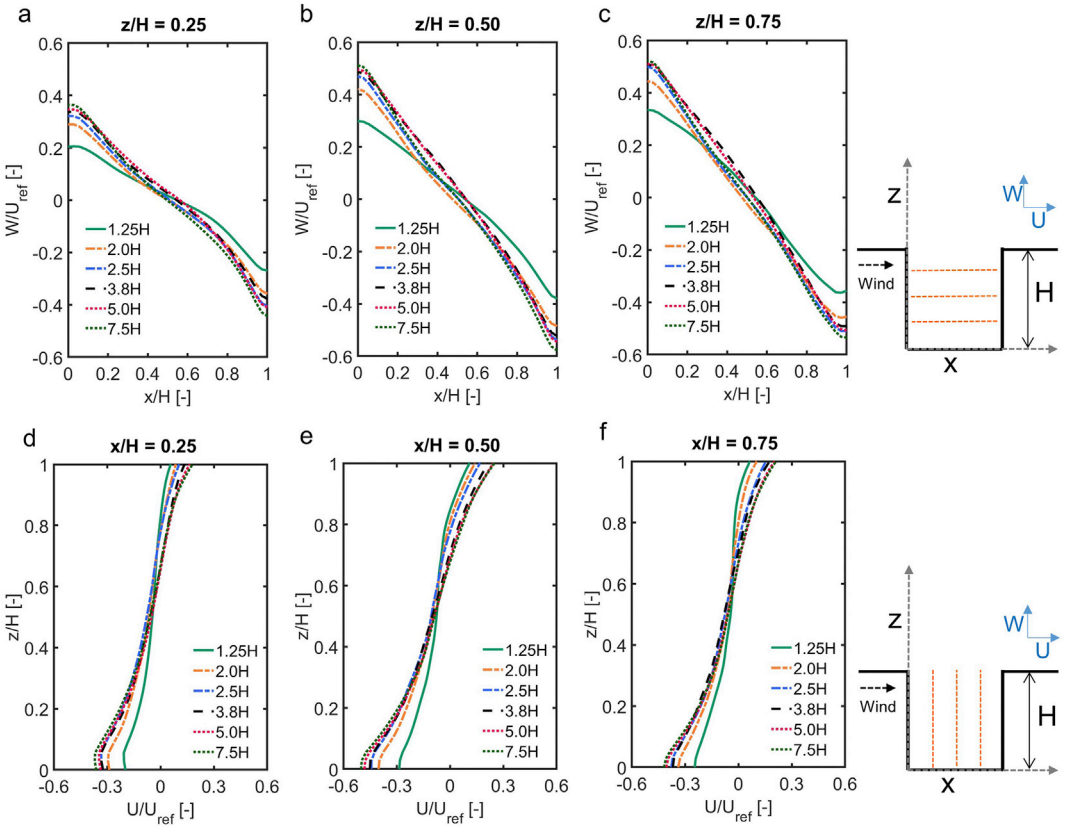

Fig. 9. Comparison of dimensionless mean velocity components obtained from six different domain widths: W/U_{ref} along three horizontal lines in the vertical centerplane: (a) z/H = 0.25; (b) z/H = 0.5; (c) z/H = 0.75, and U/U_{ref} along three vertical lines in the vertical centerplane: (d) x/H = 0.25; (e) x/H = 0.5; (f) x/H = 0.75.

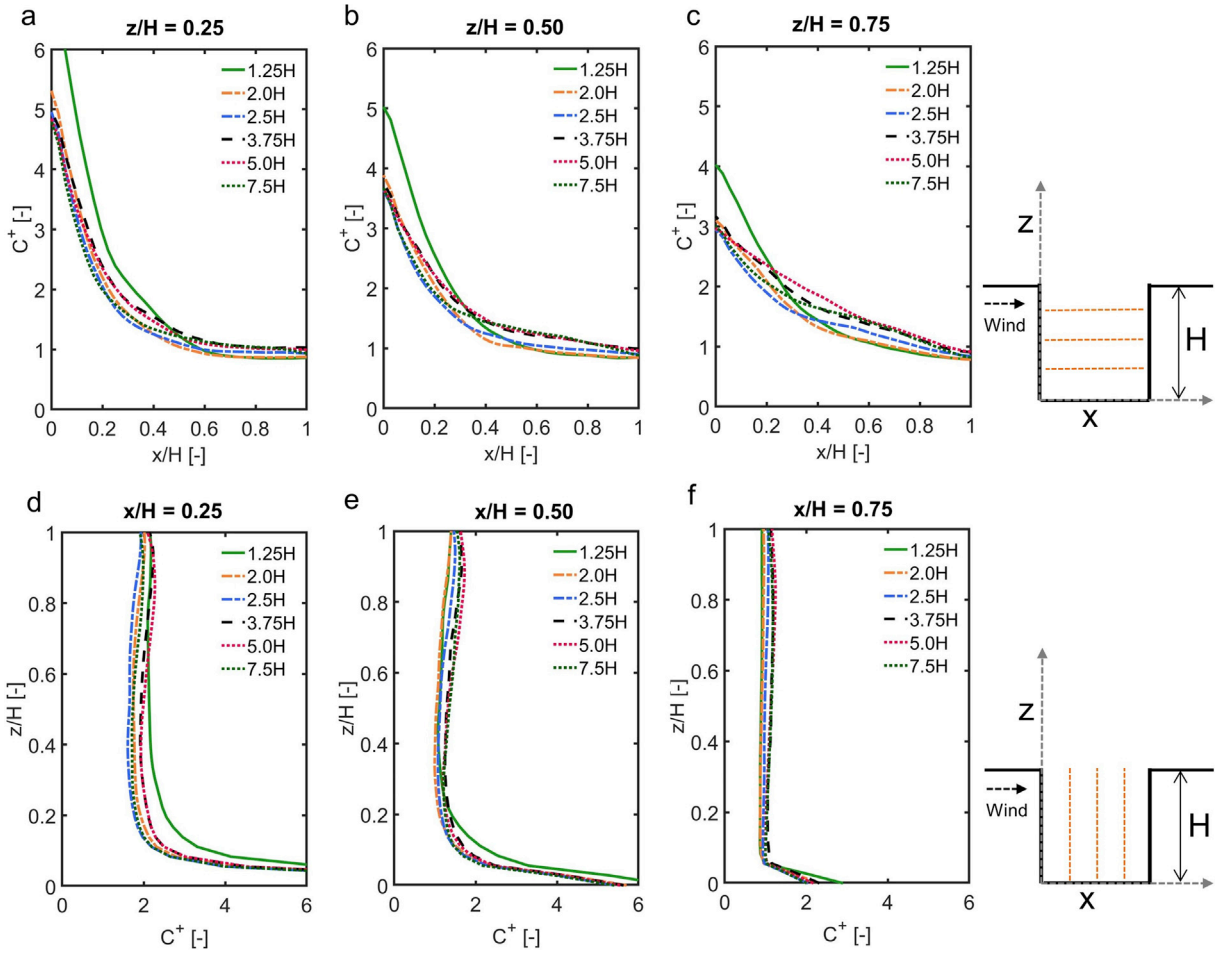

Fig. 10. Comparison of C^+ obtained from six different domain widths along three horizontal lines in the vertical centerplane: (a) z/H = 0.25; (b) z/H = 0.5; (c) z/H = 0.75, and three vertical lines in the vertical centerplane: (d) x/H = 0.25; (e) x/H = 0.5; (f) x/H = 0.75.

domain length (D_d) of 10H. Through a systematic variation of W_d, H_d, U_d and D_d, the effect of these four parameters on the simulation results is investigated. In total, 16 LES simulations are performed and the details are given in Table 3. Note that the values of W_d and H_d cover the ranges of those used in previous studies (as listed in Table 1), while those of U_d and D_d include extensions based on the validation study and guidelines (Tominaga et al., 2008). Non-conformal grids (Iousef et al., 2017) are generated. They consist of two subdomains and subgrids (Ω_1 and Ω_2), with a grid refinement ratio of 1:2 between the adjacent subgrids. Subdomain Ω_1 is composed of cubic cells with edge length H/40, similar to the grid for the validation study in Subsection 2.2. Subdomain Ω_1 extends up to a distance of H away from the building surfaces. Subdomain Ω_2 uses hexahedral cells with a stretching ratio of less than 1.05.

3.2. Boundary conditions and solver settings

The inlet mean wind speed profile is the logarithmic law (Eq. (3)) with $z_0 = 0.03$ m and $u^*_{ABL} = 0.3$ m/s. The corresponding U_{ref} at the roof height is 4.28 m/s. Turbulent kinetic energy (k) and turbulence dissipation rate (ε) are given by Eqs. (4) and (2), respectively (Richards and Hoxey, 1993). Periodic boundary conditions are applied at the lateral domain sides. At the outlet plane, zero static gauge pressure is applied. At the top of the domain, symmetry conditions are imposed, i.e. zero normal velocity and zero normal gradients of all variables. Tracer gas SF_6 representing the traffic exhaust is released from two continuous line sources that are parallel to the street axis and embedded at the street bottom surface. The width of each line source is 0.9 m and the center of each line is at a distance of 3.45 m to the nearest building wall (Fig. 7). The emission rate of tracer gas source per unit length is set as Q/l = 10 $g{\cdot}s^{-1}m^{-1}$.

$$U(z) = \frac{u^*_{ABL}}{\kappa} \ln\left(\frac{z + z_0}{z_0}\right) \tag{3}$$

$$k(z) = \frac{{u^*_{ABL}}^2}{0.3} \tag{4}$$

For the LES simulations, the WALE model is used. The vortex method is adopted to impose a time-dependent velocity profile at the inlet of the domain. The number of vortices is estimated in the same way as in the validation study. The other computational settings are identical to those in the validation study in Subsection 2.3. The time step (Δt) is 0.024 s. For the reference case, the maximum and volume-averaged Courant-Friedrichs-Lewy (CFL) numbers are 0.84 and 0.10, respectively. For the other cases, the maximum CFL number is below 1. The LES simulations are initialized from the solution of RANS simulations. Before averaging, the simulations are run during 650 s (approximately 10 flow-through times) to remove the influence of the initial condition. Then, data are averaged over a period of 1920 s (80,000 time steps, approximately 30 flow-through times).

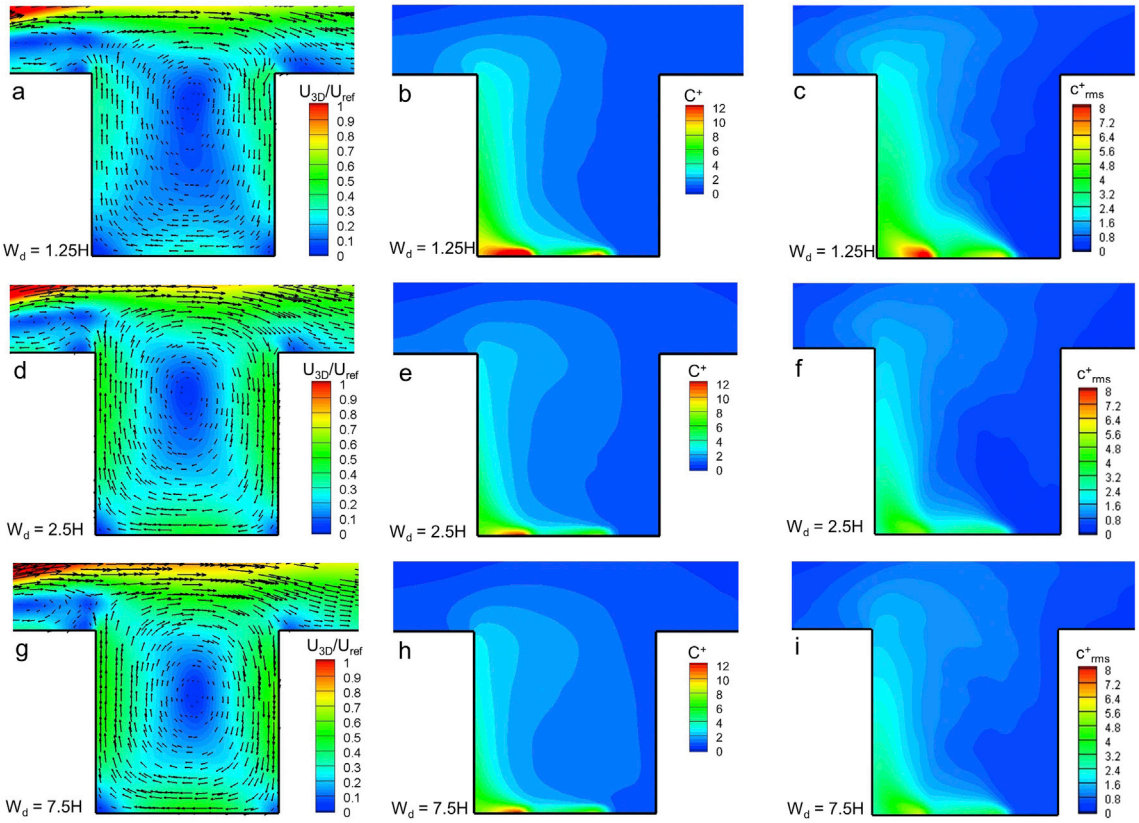

Fig. 11. (a) Distribution of U_{3D}/U_{ref} and 2D velocity vector field, (b) C^+, and (c) c^+_{rms} by the domains with $W_d = 1.25$, (d–f) $W_d = 2.5H$, and (g–i) $W_d = 7.5H$ in the vertical centerplane.

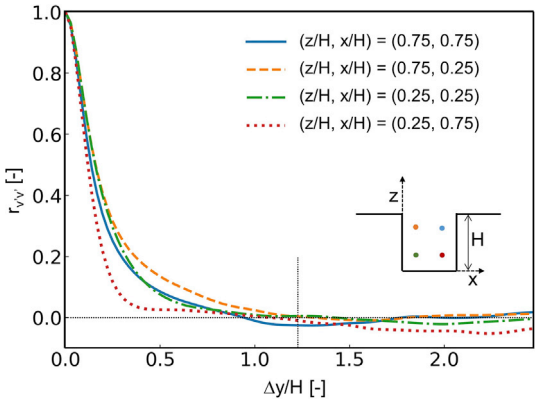

Fig. 12. Spanwise two-point correlation coefficient $r_{v'v'}$ along four lines.

3.3. Monitoring of statistical convergence

Fig. 8 shows the evolution of the moving average of dimensionless SF_6 concentration and dimensionless velocity magnitude as a function of time at five monitoring points inside the street canyon. It should be noted that to evaluate the statistical convergence of the simulation, the results are provided for approximately 45 flow-through times. It appears that the variations of the mean concentration and velocity magnitude are relatively low after about 60,000 time steps. Small variations are observed in the second half of the averaging period, which could be due to the instability of the re-circulation vortex inside the street canyon induced by the shear layer shed from the upstream roof (Louka et al., 2000; Perret and Savory, 2013; Zhang et al., 2011). The convergence of the mean value is further quantified by e_{conv} (%) defined for a given range of time steps I as follows:

$$e_{conv}(I) = \frac{|Q_{max} - Q_{min}|}{|Q_{end}|} \times 100\% \quad (5)$$

where Q_{max} and Q_{min} are the maximum and minimum values, respectively, of a flow variable obtained within an interval I of time steps in the averaging period. Q_{end} is the value of a flow variable at the end of interval I. The 120,000 time steps of the averaging period are divided into twelve equal intervals for which the values of e_{conv} are calculated for both the dimensionless mean concentration (C^+) and dimensionless mean velocity magnitude (U_{3D}/U_{ref}). Table 4 shows the results for the five monitoring points. A strong influence of the instantaneous flow patterns on the mean concentration can be observed at the beginning of the averaging period (I = 1). In this case, the value of e_{conv} goes up to 141.62%. The maximum e_{conv} reduces to 1.73% for the interval I = 12 (after approximately 45 flow-through times). Note that for interval I = 8, e_{conv} is equal to or smaller than 5.54%, which indicates a good statistical convergence of the simulation.

4. Sensitivity analysis: impact of domain width

Fig. 9 compares the dimensionless mean vertical (W/U_{ref}) and streamwise (U/U_{ref}) velocity components along the three horizontal and three vertical lines. The domain with $W_d/H = 1.25$ clearly yields lower values than the others. The domain with $W_d/H = 2.0$ predicts slightly lower mean velocity components than the wider domains. Compared to the domain with $W_d/H = 7.5$ (the largest domain width), the average absolute differences of the dimensionless mean velocity magnitude (U_{3D}/U_{ref}) along the sampling lines are 0.091, 0.043, 0.020, 0.028 and 0.020 for domains with $W_d/H = 1.25$, 2.0, 2.5, 3.75 and 5, respectively.

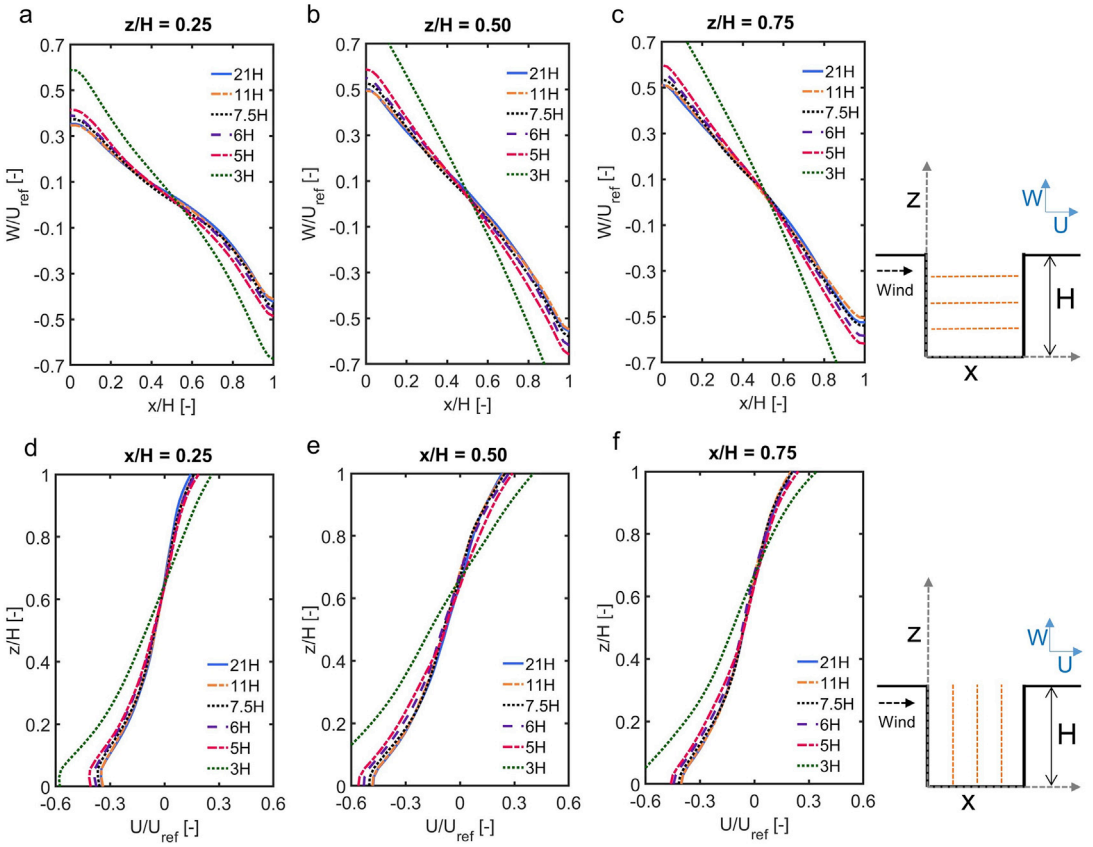

Fig. 13. Comparison of dimensionless mean velocity components obtained from six different domain heights: W/U_{ref} along three horizontal lines in the vertical centerplane (a) z/H = 0.25; (b) z/H = 0.5; (c) z/H = 0.75, and U/U_{ref} along three vertical lines in the vertical centerplane (d) x/H = 0.25; (e) x/H = 0.5; (f) x/H = 0.75.

Fig. 10 compares C^+ along the same vertical and horizontal lines, as obtained by the domains with different W_d. The domain with $W_d/H = 1.25$ predicts larger C^+ values than the other domains near the leeward wall (see Fig. 10d). For the C^+ along the horizontal lines, a different trend is predicted by the domain with $W_d/H = 1.25$ compared to the other domains (Fig. 10a–c). The domains with $W_d/H = 2$, 2.5, 3.75, 5 and 7.5 generally predict similar values for C^+. Compared to the results from the domain with the largest W_d, i.e. $W_d/H = 7.5$, the average absolute differences of the C^+ along all the lines are 0.441, 0.197, 0.119, 0.122 and 0.130 for the domains with $W_d/H = 1.25$, 2.0, 2.5, 3.75 and 5, respectively.

These results indicate that when the domain width is equal to or greater than 2.5H, the results in terms of mean velocity components and mean concentration within the street canyon become similar.

Fig. 11 displays the distribution of the dimensionless mean velocity magnitude (U_{3D}/U_{ref}) and the 2D velocity vector field, the mean concentration (C^+) and the dimensionless root mean square error concentration (c^+_{rms}) in the vertical centerplane by the domains with $W_d/H = 1.25$, 2.5 and 7.5. It is obvious that the domain with $W_d/H = 1.25$ predicts a lower mean wind velocity and weaker vortex flow within the street canyon than the other two cases. This is because the domain width is too small to include the important coherent eddies occurring in the spanwise direction, which will be evaluated later. It leads to a higher C^+ near the leeward side than the other two domains. Small differences of the C^+ between the domains with $W_d/H = 2.5$ and 7.5 are found. In terms of c^+_{rms}, the domains with $W_d/H = 2.5$ and 7.5 also yield similar results, while $W_d/H = 1.25$ predicts much higher c^+_{rms} near the leeward side.

Earlier studies have indicated that the domain width needs to be large enough to include the important and largest coherent eddies occurring in the spanwise direction (Moin and Kim, 1982; Walton and Cheng, 2002). We adopted the approach of computing the temporal correlations between two probe points on the same spanwise-oriented line to evaluate the adequacy of the domain width (Kitsios et al., 2011; Moin and Kim, 1982). Following the past study (Kitsios et al., 2011), the correlation coefficient of the fluctuation of the spanwise velocity component (y-direction), v′, between the two points is:

$$r_{v'v'}(\Delta y) = \frac{\overline{v'(y,\ t)\ v'(y\ +\ \Delta y,\ t)}}{v'_{rms}(y)\ v'_{rms}(y\ +\ \Delta y)} \tag{6}$$

where the overbar denotes temporal averaging, Δy is the spanwise separation distance between the two points on the same line, and v'_{rms} is the root mean square error of the spanwise velocity component. The correlation coefficients $r_{v'v'}$ are averaged over the combinations of two points on the same line with the same value of Δy. If the velocity components in the periodic direction (v) become uncorrelated (e.g. the correlation coefficient decays to zero) within a separation distance of half the domain size in that direction, then the domain size can be considered to be sufficiently large (Fröhlich et al., 2005).

Based on the result from the reference domain ($W_d/H = 5$, $H_d/H = 11$, $U_d/H = 10$ and $D_d/H = 10$), the two-point correlation along the four lines in the spanwise direction (y) is shown in Fig. 12. The slow decay of $r_{v'v'}$ with Δy along the line of (z/H, x/H) = (0.75, 0.25) indicates that eddies close to the top and leeward region are highly elongated in the spanwise direction. The result along the line of (z/H, x/H) = (0.25, 0.75) shows that the spanwise extent of turbulence structures near the leeward wall close to the ground is much smaller than the others. All correlation coefficients decay to zero when Δy/H reaches about 1.2, which means that W_d/H should be larger than 2.4. Considering that the domains with $W_d/H \geq 2.5$ yield similar mean concentration and mean velocity

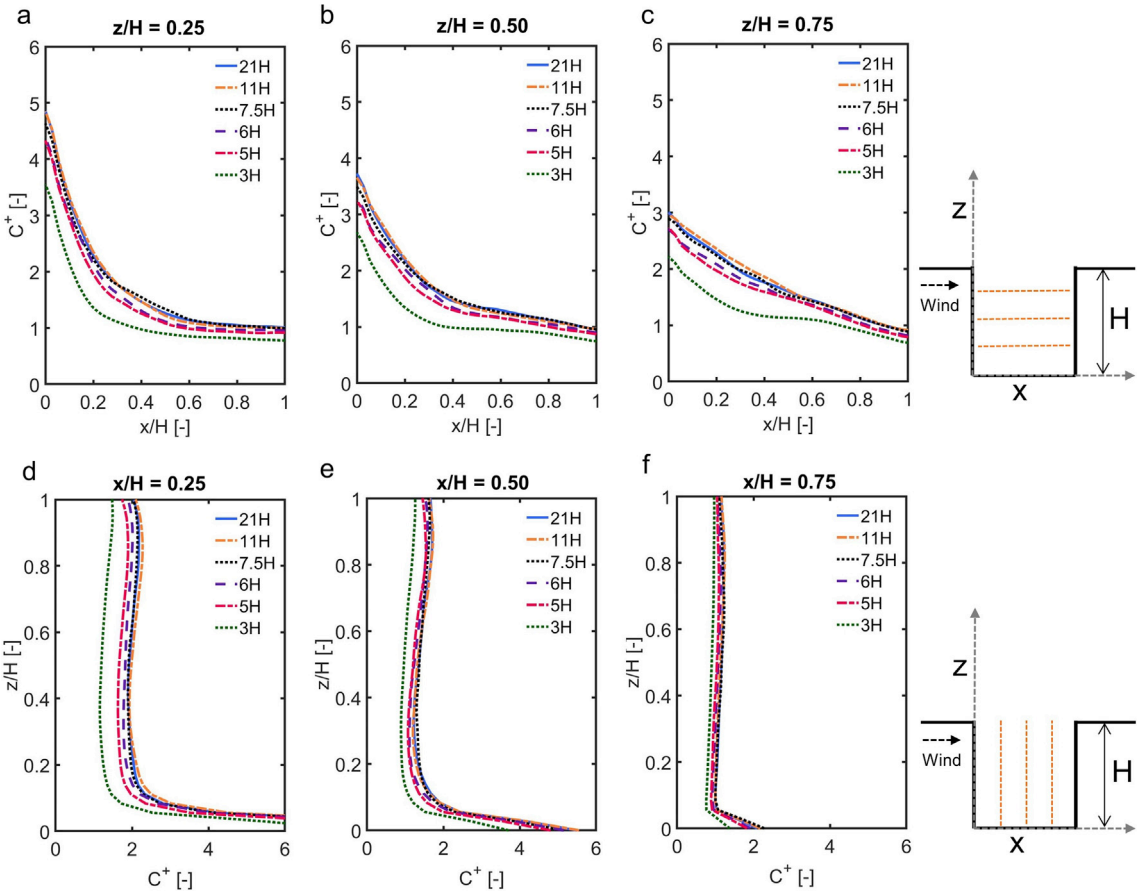

Fig. 14. Comparison of C^+ obtained from six different domain heights along three horizontal lines in the vertical centerplane: (a) z/H = 0.25; (b) z/H = 0.5; (c) z/H = 0.75, and three vertical lines in the vertical centerplane: (d) x/H = 0.25; (e) x/H = 0.5; (f) x/H = 0.75.

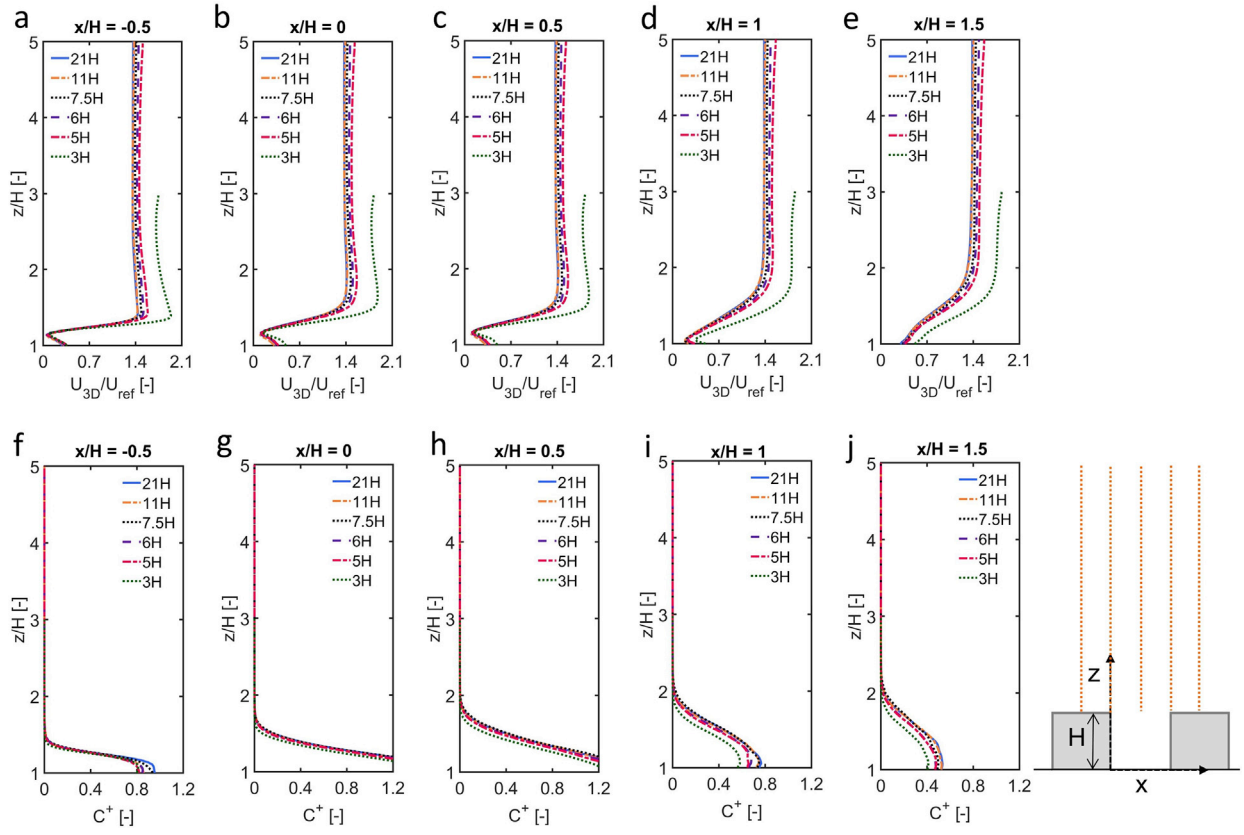

Fig. 15. Comparison of U_{3D}/U_{ref} obtained from six different domain heights along five vertical lines above the canyon in the vertical centerplane: (a) x/H = −0.5; (b) x/H = 0; (c) x/H = 0.5; (d) x/H = 1; (e) x/H = 1.5; (f–j) same for C^+.

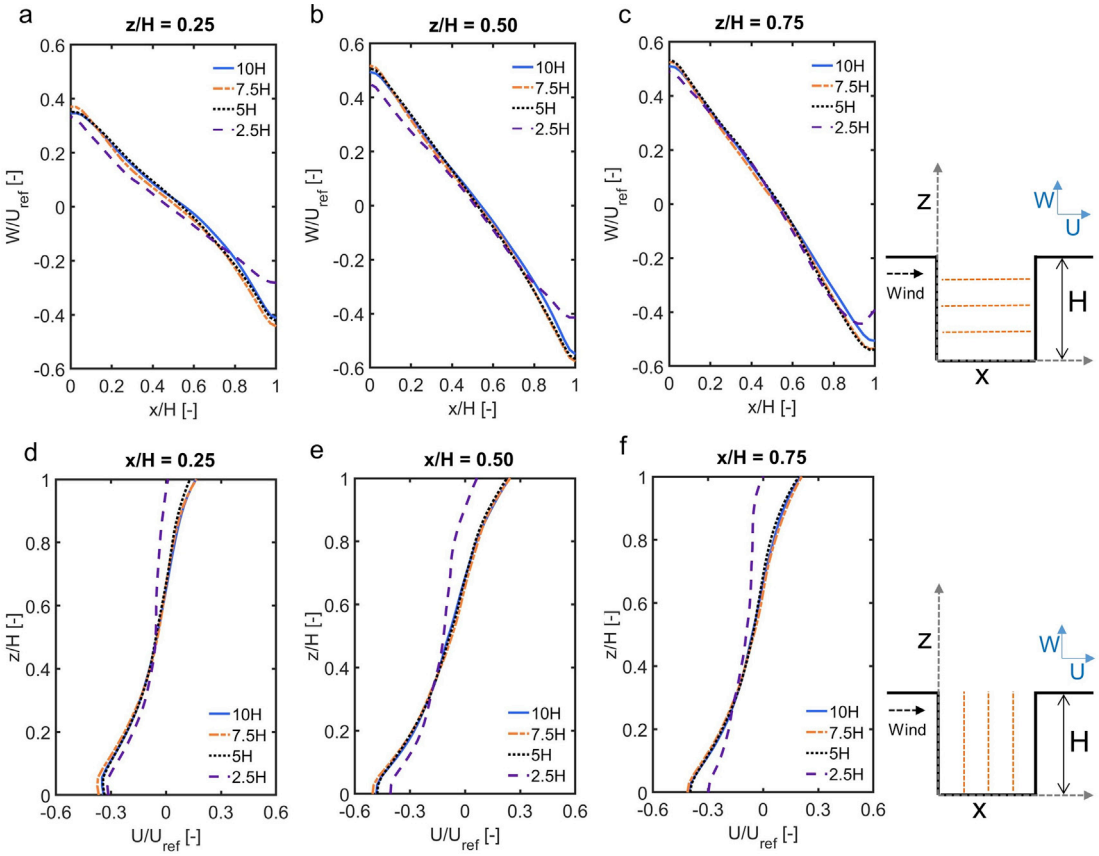

Fig. 16. Comparison of dimensionless mean velocity components obtained by four different upstream domain lengths: W/U_{ref} along three horizontal lines in the vertical centerplane (a) z/H = 0.25; (b) z/H = 0.5; (c) z/H = 0.75, and U/U_{ref} along three vertical lines in the vertical centerplane (d) x/H = 0.25; (e) x/H = 0.5; (f) x/H = 0.75.

components, $W_d/H = 2.5$ can be considered as the minimum requirement of the domain width.

5. Sensitivity analysis: impact of domain height

Fig. 13 displays W/U_{ref} and U/U_{ref} along the three horizontal lines and three vertical lines in the vertical centerplane obtained using six different domain heights. It shows that the blockage due to the presence of the building in the domain results in an artificial acceleration of the flow within the canyon. A monotonic and asymptotic increase of mean velocity components is found with a decrease of domain height. Compared to the domain with $H_d/H = 21$ (the largest domain height), the average absolute differences of the dimensionless mean velocity magnitude (U_{3D}/U_{ref}) along the sampling lines are 0.196, 0.052, 0.030, 0.014 and 0.007 for domains with H_d/H = 3, 5, 6, 7.5 and 11, respectively.

Fig. 14 compares the profiles of C^+ along the same horizontal and vertical lines for the six domain heights. For the domains with H_d/H = 7.5, 11 and 21, negligible differences are observed for the predicted C^+, while for the domains with H_d/H = 3, 5 and 6, C^+ is systematically underpredicted. Compared to the domain with $H_d/H = 21$ (the largest domain height), the average absolute differences of C^+ along all sampling lines for the domains with H_d/H = 3, 5, 6, 7.5 and 11 are 0.546, 0.218, 0.141, 0.047 and 0.042, respectively.

Fig. 15 shows the dimensionless mean velocity magnitude (U_{3D}/U_{ref}) and dimensionless mean concentration (C^+) along five vertical lines above the canyon in the vertical centerplane, as obtained from the six different domain heights. It is observed that the shear layer thickness increases when moving downstream. For the mean velocity within and below the shear layer, the largest value is achieved for the domain with $H_d/H = 3$ (Fig. 15a–e). For the mean wind velocity in the free stream flow, a monotonic increase is found with the decrease of the domain height. For C^+ within and below the shear layer, the domain with H_d/H = 3 predicts lower C^+ than the other five domains (see Fig. 15i and j).

The effect of the domain height on the mean wind velocity inside and in the vicinity of the street canyon is negligible when H_d/H is equal to or greater than 7.5 (Figs. 13 and 15). The results of C^+ also indicate that the domain with H_d/H equal to or larger than 7.5 shows relatively similar results, and the smaller domain height (H_d) clearly yields larger C^+ (Figs. 14 and 15). These imply that a blockage ratio of 13.3% is sufficient to avoid the impact of flow acceleration on the results inside and around the street canyon.

6. Sensitivity analysis: impact of domain lengths

Fig. 16 shows W/U_{ref} and U/U_{ref} along the three horizontal lines and three vertical lines in the vertical centerplane obtained using four different upstream domain lengths. Fig. 17 displays C^+ along the same lines. It indicates that domain with $U_d/H = 2.5$ clearly yields lower values of W/U_{ref}, U/U_{ref}, and C^+ compared with the other domains, while U_d/H = 5, 7.5 and 10 show relatively similar results. Based on the large discrepancies, the use of U_d/H below 5 is not recommended. This is consistent with the guidelines (Franke et al., 2011) that the inlet boundary should be at least $5H_{max}$ to the building.

Fig. 18 displays W/U_{ref} and U/U_{ref} along the three horizontal lines and three vertical lines, as obtained using three different downstream domain lengths. The mean velocity components predicted by the domain with $U_d/H = 3$ are smaller than those by the other domains.

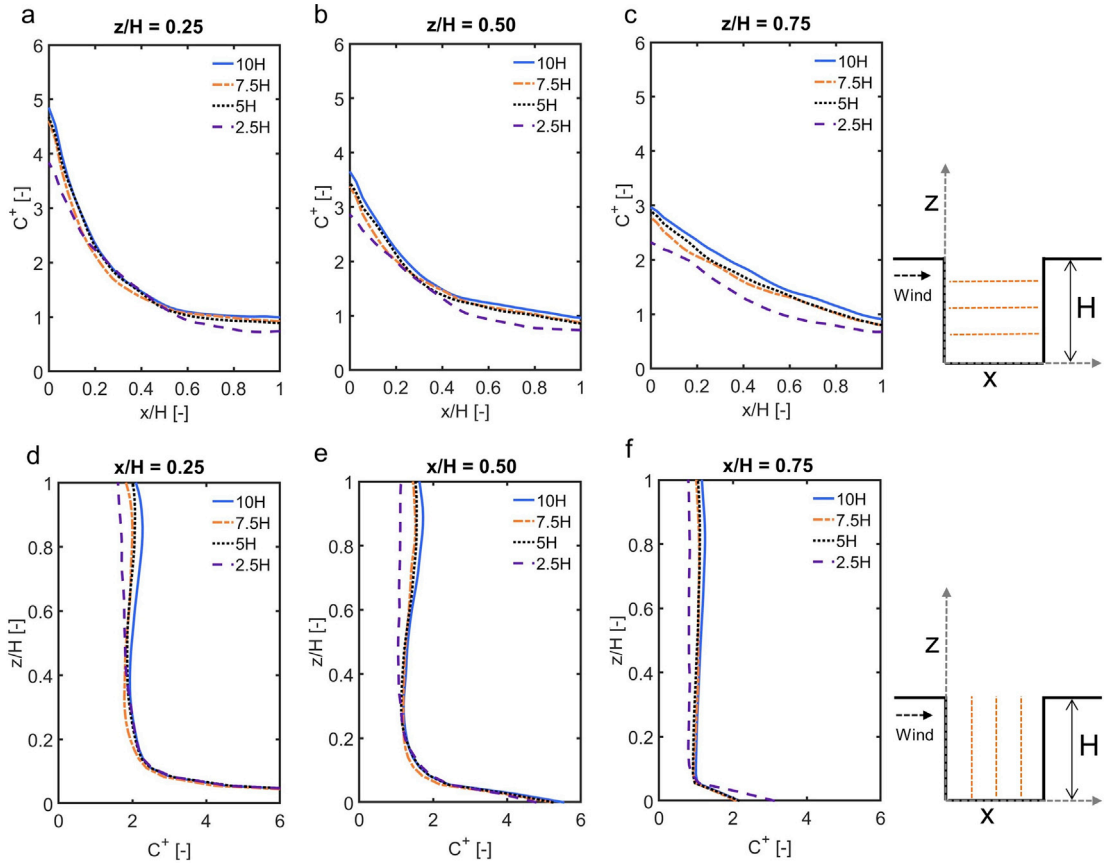

Fig. 17. Comparison of C^+ obtained from four different upstream domain lengths along three horizontal lines in the vertical centerplane: (a) z/H = 0.25; (b) z/H = 0.5; (c) z/H = 0.75; and three vertical lines in the vertical centerplane: (d) x/H = 0.25; (e) x/H = 0.5; (f) x/H = 0.75.

Fig. 19 displays C^+ along the same lines. Relatively large differences between the three domains are observed. During the simulation for domains with $D_d/H = 3$ and 6, reversed flow in large numbers of faces is reported in the outlet plane, which is not in line with recommendations by the best practice guidelines for CFD simulations of wind flow in urban areas (Franke et al., 2007). Guidelines for all applications of urban flow (Tominaga et al., 2008) indicated that the outflow boundary is recommended to be at least $10H_{max}$ away from the building group. Therefore, we also recommend 10H for this type of simulation.

7. Discussion

The present finding of the blockage ratio is smaller than the recommended directional blockage ratio (Blocken, 2015) (i.e. about 17%). However, when compared with the full blockage ratio by best practice guidelines for urban flows (Blocken, 2015; Franke et al., 2011; Tominaga et al., 2008), i.e. maximum blockage ratio of 3%, the present finding of the blockage ratio is much larger. The possible reason for these differences is that best practice guidelines for urban flows were developed to avoid artificial accelerations occurring at both the top and sides of buildings. In the present study, the street canyon is simulated as 2.5D without considering the airflow near the sides of buildings but only focusing on the airflow and concentration inside the canyon.

The case evaluated in the present study is limited to a simple street canyon with the aspect ratio (= H/W) of 1, which is the common generic street canyon found in the literature (Table 1). As shown by the two-point correlation and the comparison of the mean velocity components and mean concentration in Section 4, the domain width needs to be large enough to include the important coherent eddies occurring in the spanwise direction. In this perspective, the spanwise extent of turbulence structures within street canyons is important. A recent experimental study investigated the effect of the upstream roughness and aspect ratio on the spanwise structure of the roof-level turbulence in long uniform street canyons (Jaroslawski et al., 2019a, 2019b). The results indicated that canyons with a large aspect ratio have large-scale vortex organization in the spanwise direction (Jaroslawski et al., 2019a). It also demonstrated that the upstream roughness and the aspect ratio have significant effects on the spanwise turbulence integral length at the roof-level (Jaroslawski et al., 2019b). The turbulence at the roof-level may affect the spanwise turbulence within the canyon. Therefore, it is important to highlight that the aforementioned minimum domain size in Section 4 is recommended for 1:1 single street canyon cases exposed to an atmospheric boundary layer, which may not be valid for other cases.

As shown by past studies (Montazeri and Blocken, 2013; Montazeri et al., 2013; Stathopoulos and Zhu, 1988; Zheng et al., 2020), the presence of building facade geometrical details such as balconies may introduce a high level of complexity in the airflow. Therefore, the domain width obtained in the present study may not be valid for cases with façade geometrical details. Further studies should focus on cases with upstream obstacles, with multiple street canyons in sequence, with other aspect ratios, and with façade geometrical details.

8. Conclusions and recommendations

The current study evaluated the influence of the domain width, domain height, and upstream and downstream domain lengths on the prediction of the wind field and pollutant dispersion in generic single street canyons. The study has led to a set of conclusions and

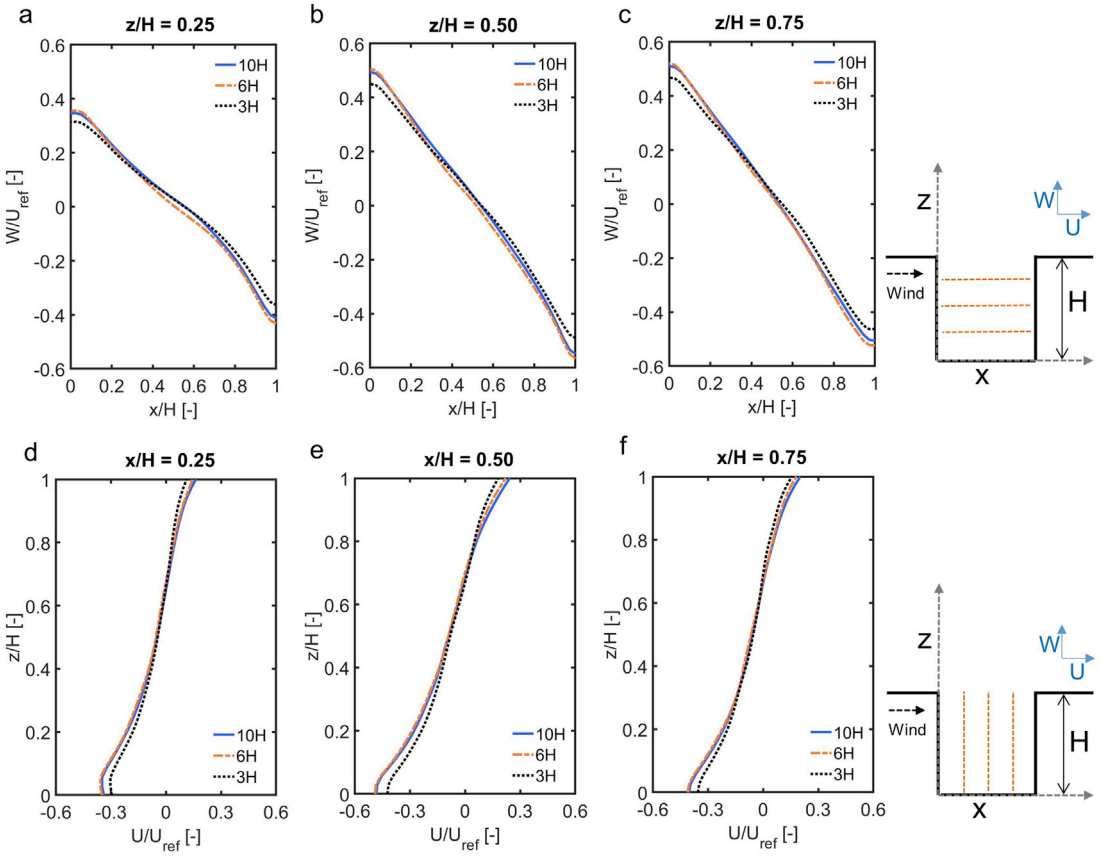

Fig. 18. Comparison of dimensionless mean velocity components obtained from three different downstream domain lengths: W/U_{ref} along three horizontal lines in the vertical centerplane (a) z/H = 0.25; (b) z/H = 0.5; (c) z/H = 0.75, and U/U_{ref} along three vertical lines in the vertical centerplane (d) x/H = 0.25; (e) x/H = 0.5; (f) x/H = 0.75.

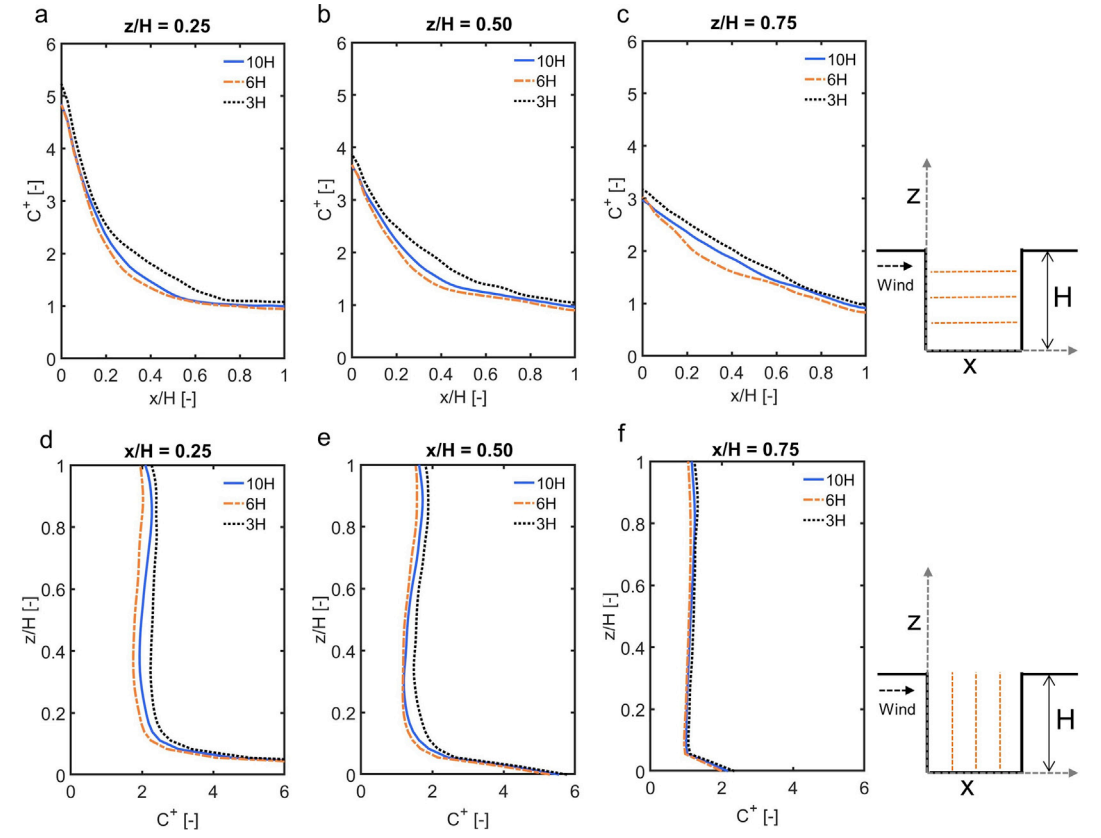

Fig. 19. Comparison of C^+ obtained from three different downstream domain lengths along three horizontal lines in the vertical centerplane: (a) z/H = 0.25; (b) z/H = 0.5; (c) z/H = 0.75, and three vertical lines in the vertical centerplane: (d) x/H = 0.25; (e) x/H = 0.5; (f) x/H = 0.75.

recommendations towards the application of LES simulation for a 2.5D street canyon with spanwise periodic boundary conditions. The following conclusions aim at reducing the size of the computational domain without significantly compromising the accuracy:

(1) Compared to the domain with $W_d/H = 7.5$ (the largest domain width), the average absolute differences between the dimensionless mean velocity magnitude (U_{3D}/U_{ref}) along the sampling lines by domains with $W_d/H = 1.25$, 2.0, 2.5, 3.75 and 5 are 0.091, 0.043, 0.020, 0.028 and 0.020, respectively. The differences for the C^+ are 0.441, 0.197, 0.119, 0.122 and 0.130, respectively. It indicates that when the domain width is equal to or greater than 2.5H, a similarity of results in terms of mean velocity and mean concentration within the street canyon is obtained. The two-point correlation analysis indicates that the domain width should be larger than 2.4H. As a result, this study recommends the minimum safe value of 2.5H.
(2) Compared to the domain with $H_d/H = 21$ (the largest domain height), the average absolute differences of the dimensionless mean velocity magnitude along the sampling lines for domains with $H_d/H = 3$, 5, 6, 7.5 and 11 are 0.196, 0.052, 0.030, 0.014 and 0.007, respectively. These differences for the C^+ are 0.546, 0.218, 0.141, 0.047 and 0.042, respectively. The domain height of 7.5H is recommended to minimize the effect of the blockage effect. This is equivalent to a blockage ratio of 13.3%. Smaller domain height can result in the overprediction of mean velocity and underprediction of mean concentration.
(3) For the upstream domain length (U_d) and downstream domain length (D_d), the present findings are consistent with the existing guidelines for RANS simulations, with minimum values for U_d and D_d equal to 5H and 10H, respectively.

CRediT authorship contribution statement

Xing Zheng: Formal analysis, Investigation, Writing - review & editing, Writing - original draft, Data analysis, numerical Investigation, data and text editing, writing - original draft. **Hamid Montazeri:** Supervision, Writing - review & editing, Writing - original draft, Supervision, writing, text editing, revising. **Bert Blocken:** Supervision, Writing - review & editing, Writing - original draft, Funding acquisition, Supervision, writing, text editing, revising, funding acquisition.

Declaration of competing interest

The authors declare that they have no known competing financial interests or personal relationships that could have appeared to influence the work reported in this paper.

Acknowledgments

This work has been sponsored by NWO Exacte en Natuurwetenschappen (Physical Sciences) for the use of supercomputer facilities, with financial support from the Nederlandse Organisatie voor Wetenschappelijk Onderzoek (Netherlands Organization for Scientific Research, NWO). The authors would like to express sincere thanks to Dr. Christof Bernhard Gromke for his comments and advice. The authors also gratefully acknowledge the partnership with ANSYS CFD.

References

Ai, Z.T., Mak, C.M., 2017. CFD simulation of flow in a long street canyon under a perpendicular wind direction: evaluation of three computational settings. Build. Environ. 114, 293–306. https://doi.org/10.1016/j.buildenv.2016.12.032.
Ai, Z.T., Mak, C.M., 2015. Large-eddy Simulation of flow and dispersion around an isolated building: analysis of influencing factors. Comput. Fluids 118, 89–100. https://doi.org/10.1016/j.compfluid.2015.06.006.
Ansys Inc, 2017. Release 18.0, Theory Guide. ANSYS Inc, Canonsburg, PA 15317, USA.
Antoniou, N., Montazeri, H., Neophytou, M., Blocken, B., 2019. CFD simulation of urban microclimate: validation using high-resolution field measurements. Sci. Total Environ. 695, 133743. https://doi.org/10.1016/j.scitotenv.2019.133743.
Antoniou, N., Montazeri, H., Wigo, H., Neophytou, M.K.-A., Blocken, B., Sandberg, M., 2017. CFD and wind-tunnel analysis of outdoor ventilation in a real compact heterogeneous urban area: evaluation using "air delay. Build. Environ. 126, 355–372. https://doi.org/10.1016/j.buildenv.2017.10.013.
Baik, J.-J., Kwak, K.-H., Park, S.-B., Ryu, Y.-H., 2012. Effects of building roof greening on air quality in street canyons. Atmos. Environ. 61, 48–55. https://doi.org/10.1016/j.atmosenv.2012.06.076.
Baker, J., Walker, H.L., Cai, X., 2004. A study of the dispersion and transport of reactive pollutants in and above street canyons—a large eddy simulation. Atmos. Environ. 38, 6883–6892. https://doi.org/10.1016/j.atmosenv.2004.08.051.
Baratian-Ghorghi, Z., Kaye, N.B., 2013. The effect of canyon aspect ratio on flushing of dense pollutants from an isolated street canyon. Sci. Total Environ. 443, 112–122. https://doi.org/10.1016/j.scitotenv.2012.10.064.
Blocken, B., 2018. LES over RANS in building simulation for outdoor and indoor applications: a foregone conclusion? Build. Simul. https://doi.org/10.1007/s12273-018-0459-3.
Blocken, B., 2015. Computational Fluid Dynamics for urban physics: importance, scales, possibilities, limitations and ten tips and tricks towards accurate and reliable simulations. Build. Environ. 91, 219–245. https://doi.org/10.1016/j.buildenv.2015.02.015.
Bright, V.B., Bloss, W.J., Cai, X., 2013. Urban street canyons: coupling dynamics, chemistry and within-canyon chemical processing of emissions. Atmos. Environ. 68, 127–142. https://doi.org/10.1016/j.atmosenv.2012.10.056.
Buccolieri, R., Gromke, C., Di Sabatino, S., Ruck, B., 2009. Aerodynamic effects of trees on pollutant concentration in street canyons. Sci. Total Environ. 407, 5247–5256. https://doi.org/10.1016/j.scitotenv.2009.06.016.
Chatzimichailidis, A.E., Argyropoulos, C.D., Assael, M.J., Kakosimos, K.E., 2019. Qualitative and quantitative investigation of multiple large eddy simulation aspects for pollutant dispersion in street canyons using OpenFOAM. Atmosphere 10. https://doi.org/10.3390/atmos10010017.
Cheng, W.C., Liu, C.-H., 2011. Large-eddy simulation of turbulent transports in urban street canyons in different thermal stabilities. J. Wind Eng. Ind. Aerod. 99, 434–442. https://doi.org/10.1016/j.jweia.2010.12.009.
Chew, L.W., Glicksman, L.R., Norford, L.K., 2018. Buoyant flows in street canyons: comparison of RANS and LES at reduced and full scales. Build. Environ. 146, 77–87. https://doi.org/10.1016/j.buildenv.2018.09.026.
Ding, S., Huang, Y., Cui, P., Wu, J., Li, M., Liu, D., 2019. Impact of viaduct on flow reversion and pollutant dispersion in 2D urban street canyon with different roof shapes - numerical simulation and wind tunnel experiment. Sci. Total Environ. 671, 976–991. https://doi.org/10.1016/j.scitotenv.2019.03.391.
Duan, G., Ngan, K., 2018. Effects of time-dependent inflow perturbations on turbulent flow in a street canyon. Boundary-Layer Meteorol. 167, 257–284. https://doi.org/10.1007/s10546-017-0327-1.
Ducros, F., Nicoud, F., Poinsot, T., 1998. Wall-adapting local eddy-viscosity models for simulations in complex geometries. In: Oxford University Computing Laboratory. 16th Conference on Numerical Methods in Fluid Dynamics, Arcachon, France, pp. 293–299.
Franke, J., Hellsten, A., Schlunzen, H., Carissimo, B., 2011. The COST 732 Best practice guideline for CFD simulation of flows in the urban environment: a summary. Int. J. Environ. Pollut. 44, 419. https://doi.org/10.1504/ijep.2011.038443.
Franke, J., Hellsten, A., Schlünzen, H., Carissimo, B., 2007. Best Practice Guideline for the CFD Simulation of Flows in the Urban Environment. Meteorological Inst., COST, Hamburg, Germany.
Fröhlich, J., Mellen, C.P., Rodi, W., Temmerman, L., Leschziner, M.A., 2005. Highly resolved large-eddy simulation of separated flow in a channel with streamwise periodic constrictions. J. Fluid Mech. 526, 19–66. https://doi.org/10.1017/S0022112004002812.
Gallagher, J., Lago, C., 2019. How parked cars affect pollutant dispersion at street level in an urban street canyon? A CFD modelling exercise assessing geometrical detailing and pollutant decay rates. Sci. Total Environ. 651, 2410–2418. https://doi.org/10.1016/j.scitotenv.2018.10.135.
Geng, F., Kalkman, I., Suiker, A.S.J., Blocken, B., 2018. Sensitivity analysis of airfoil aerodynamics during pitching motion at a Reynolds number of 1.35×105. J. Wind Eng. Ind. Aerod. 183, 315–332. https://doi.org/10.1016/j.jweia.2018.11.009.
Gerasimov, A., 2016. Quick Guide to Setting up LES-type Simulations. European Technology Group, ANSYS Sweden AB, version 1.4.
Gousseau, P., Blocken, B., Van Heijst, G.J.F., 2013. Quality assessment of Large-Eddy Simulation of wind flow around a high-rise building: validation and solution verification. Comput. Fluids 79, 120–133. https://doi.org/10.1016/j.compfluid.2013.03.006.
Gromke, C., 2008. Concentration data of street canyon. Internet database [WWW Document]. URL. http://www.codasc.de, 2008.
Gromke, C., 2008b. Einfluss von Bäumen auf die Durchlüftung von innerstädtischen Straßenschluchten. KIT Scientific Publishing.
Gromke, C., Buccolieri, R., Di Sabatino, S., Ruck, B., 2008. Dispersion study in a street canyon with tree planting by means of wind tunnel and numerical investigations – evaluation of CFD data with experimental data. Atmos. Environ. 42, 8640–8650. https://doi.org/10.1016/j.atmosenv.2008.08.019.
Gromke, C., Ruck, B., 2009. On the impact of trees on dispersion processes of traffic emissions in street canyons. Boundary-Layer Meteorol. 131, 19–34. https://doi.org/10.1007/s10546-008-9301-2.

Gromke, C., Ruck, B., 2007. Influence of trees on the dispersion of pollutants in an urban street canyon—experimental investigation of the flow and concentration field. Atmos. Environ. 41, 3287–3302. https://doi.org/10.1016/j.atmosenv.2006.12.043.
Han, B.-S., Baik, J.-J., Kwak, K.-H., Park, S.-B., 2018. Large-eddy simulation of reactive pollutant exchange at the top of a street canyon. Atmos. Environ. 187, 381–389. https://doi.org/10.1016/j.atmosenv.2018.06.012.
Hanjalic, K., 2005. Will RANS survive LES? A view of perspectives. J. Fluid Eng. 127, 831. https://doi.org/10.1115/1.2037084.
He, L., Hang, J., Wang, X., Lin, B., Li, X., Lan, G., 2017. Numerical investigations of flow and passive pollutant exposure in high-rise deep street canyons with various street aspect ratios and viaduct settings. Sci. Total Environ. 584–585, 189–206. https://doi.org/10.1016/j.scitotenv.2017.01.138.
Hu, L.H., Huo, R., Yang, D., 2009. Large eddy simulation of fire-induced buoyancy driven plume dispersion in an urban street canyon under perpendicular wind flow. J. Hazard Mater. 166, 394–406. https://doi.org/10.1016/j.jhazmat.2008.11.105.
Huang, Y.-D., Xu, X., Liu, Z.-Y., Deng, J.-T., Kim, C.-N., 2016. Impacts of shape and height of building roof on airflow and pollutant dispersion inside an isolated street canyon. Environ. Forensics 17, 361–379. https://doi.org/10.1080/15275922.2016.1230912.
Iousef, S., Montazeri, H., Blocken, B., van Wesemael, P.J.V., 2017. On the use of non-conformal grids for economic LES of wind flow and convective heat transfer for a wall-mounted cube. Build. Environ. 119, 44–61. https://doi.org/10.1016/j.buildenv.2017.04.004.
Jaroslawski, T., Perret, L., Blackman, K., Savory, E., 2019a. The spanwise variation of roof-level turbulence in a street-canyon flow. Boundary-Layer Meteorol. 170, 373–394. https://doi.org/10.1007/s10546-018-0405-z.
Jaroslawski, T., Savory, E., Perret, L., 2019b. The Characterization of the Spanwise Roof-Level Turbulence in a Street Canyon Flow. University of Western Ontario.
Kastner-Klein, P., Berkowicz, R., Britter, R., 2004. The influence of street architecture on flow and dispersion in street canyons. Meteorol. Atmos. Phys. 87, 121–131. https://doi.org/10.1007/s00703-003-0065-4.
Kastner-Klein, P., Plate, E.J., 1999. Wind-tunnel study of concentration fields in street canyons. Atmos. Environ. 33, 3973–3979. https://doi.org/10.1016/S1352-2310(99)00139-9.
Kikumoto, H., Ooka, R., 2012a. A numerical study of air pollutant dispersion with bimolecular chemical reactions in an urban street canyon using large-eddy simulation. Atmos. Environ. 54, 456–464. https://doi.org/10.1016/j.atmosenv.2012.02.039.
Kikumoto, H., Ooka, R., 2012b. A study on air pollutant dispersion with bimolecular reactions in urban street canyons using large-eddy simulations. J. Wind Eng. Ind. Aerod. 104–106, 516–522. https://doi.org/10.1016/j.jweia.2012.03.001.
Kitsios, V., Cordier, L., Bonnet, J.-P., Ooi, A., Soria, J., 2011. On the coherent structures and stability properties of a leading-edge separated aerofoil with turbulent recirculation. J. Fluid Mech. 683, 395–416. https://doi.org/10.1017/jfm.2011.285.
Lateb, M., Meroney, R.N., Yataghene, M., Fellouah, H., Saleh, F., Boufadel, M.C., 2016. On the use of numerical modelling for near-field pollutant dispersion in urban environments – A review. Environ. Pollut. 208, 271–283. https://doi.org/10.1016/j.envpol.2015.07.039.
Li, X.-X., Britter, R.E., Yong Koh, T., Norford, L.K., Liu, C.-H., Entekhabi, D., C Leung, D.Y., 2010. Large-eddy simulation of flow and pollutant transport in urban street canyons with ground heating. Boundary-Layer Meteorol. 137, 187–204. https://doi.org/10.1007/s10546-010-9534-8.
Li, X.-X., Leung, D.Y.C., Liu, C.-H., Lam, K.M., 2008a. Physical modeling of flow field inside urban street canyons. J. Appl. Meteorol. Climatol. 47, 2058–2067. https://doi.org/10.1175/2007JAMC1815.1.
Li, X.-X., Liu, C.-H., Leung, D.Y.C., 2008b. Large-eddy simulation of flow and pollutant dispersion in high-aspect-ratio urban street canyons with wall model. Boundary-Layer Meteorol. 129, 249–268. https://doi.org/10.1007/s10546-008-9313-y.
Liu, C.-H., Barth, M.C., Leung, D.Y.C., 2004. Large-eddy simulation of flow and pollutant transport in street canyons of different building-height-to-street-width ratios. J. Appl. Meteorol. 43, 1410–1424. https://doi.org/10.1175/JAM2143.1.
Llaguno-Munitxa, M., Bou-Zeid, E., 2018. Shaping buildings to promote street ventilation: a large-eddy simulation study. Urban Clim 26, 76–94. https://doi.org/10.1016/j.uclim.2018.08.006.
Llaguno-Munitxa, M., Bou-Zeid, E., Hultmark, M., 2017. The influence of building geometry on street canyon air flow: validation of large eddy simulations against wind tunnel experiments. J. Wind Eng. Ind. Aerod. 165, 115–130. https://doi.org/10.1016/j.jweia.2017.03.007.
Lo, K.W., Ngan, K., 2015. Characterising the pollutant ventilation characteristics of street canyons using the tracer age and age spectrum. Atmos. Environ. 122, 611–621. https://doi.org/10.1016/j.atmosenv.2015.10.023.
Louka, P., Belcher, S.E., Harrison, R.G., 2000. Coupling between air flow in streets and the well-developed boundary layer aloft. Atmos. Environ. 34, 2613–2621.
Mathey, F., Cokljat, D., Bertoglio, J.P., Sergent, E., 2006. Assessment of the vortex method for Large Eddy Simulation inlet conditions. Prog. Comput. Fluid Dyn. An Int. J. 6, 58. https://doi.org/10.1504/PCFD.2006.009483.
Mei, S.-J., Liu, C.-W., Liu, D., Zhao, F.-Y., Wang, H.-Q., Li, X.-H., 2016. Fluid mechanical dispersion of airborne pollutants inside urban street canyons subjecting to multi-component ventilation and unstable thermal stratifications. Sci. Total Environ. 565, 1102–1115. https://doi.org/10.1016/j.scitotenv.2016.05.150.
Merlier, L., Jacob, J., Sagaut, P., 2018. Lattice-Boltzmann large-eddy simulation of pollutant dispersion in street canyons including tree planting effects. Atmos. Environ. 195, 89–103. https://doi.org/10.1016/j.atmosenv.2018.09.040.
Meroney, R., Ohba, R., Leitl, B., Kondo, H., Grawe, D., Tominaga, Y., 2016. Review of CFD guidelines for dispersion modeling. Fluid 1, 14. https://doi.org/10.3390/fluids1020014.
Meroney, R.N., Pavageau, M., Rafailidis, S., Schatzmann, M., 1996. Study of line source characteristics for 2-D physical modelling of pollutant dispersion in street canyons. J. Wind Eng. Ind. Aerod. 62, 37–56. https://doi.org/10.1016/S0167-6105(96)00057-8.
Moin, P., Kim, J., 1982. Numerical investigation of turbulent channel flow. J. Fluid Mech. 118, 341. https://doi.org/10.1017/S0022112082001116.
Montazeri, H., Blocken, B., 2013. CFD simulation of wind-induced pressure coefficients on buildings with and without balconies: validation and sensitivity analysis. Build. Environ. 60, 137–149. https://doi.org/10.1016/j.buildenv.2012.11.012.
Montazeri, H., Blocken, B., Janssen, W.D., van Hooff, T., 2013. CFD evaluation of new second-skin facade concept for wind comfort on building balconies: case study for the Park Tower in Antwerp. Build. Environ. 68, 179–192. https://doi.org/10.1016/j.buildenv.2013.07.004.
Moonen, P., Dorer, V., Carmeliet, J., 2011. Evaluation of the ventilation potential of courtyards and urban street canyons using RANS and LES. Jnl. Wind Eng. Ind. Aerodyn. 99, 414–423. https://doi.org/10.1016/j.jweia.2010.12.012.
Moonen, P., Gromke, C., Dorer, V., 2013. Performance assessment of Large Eddy Simulation (LES) for modeling dispersion in an urban street canyon with tree planting. Atmos. Environ. 75, 66–76. https://doi.org/10.1016/j.atmosenv.2013.04.016.
Nosek, Š., Kukačka, L., Jurčáková, K., Kellnerová, R., Jaňour, Z., 2017. Impact of roof height non-uniformity on pollutant transport between a street canyon and intersections. Environ. Pollut. 227, 125–138. https://doi.org/10.1016/j.envpol.2017.03.073.
O'Neill, J.J., Cai, X.-M., Kinnersley, R., 2016. Stochastic backscatter modelling for the prediction of pollutant removal from an urban street canyon: a large-eddy simulation. Atmos. Environ. 142, 9–18. https://doi.org/10.1016/j.atmosenv.2016.07.024.
Oke, T.R., 1988. Street design and urban canopy layer climate. Energy Build. 11, 103–113. https://doi.org/10.1016/0378-7788(88)90026-6.
Park, S.-B., Baik, J.-J., Raasch, S., Letzel, M.O., 2012. A large-eddy simulation study of thermal effects on turbulent flow and dispersion in and above a street canyon. J. Appl. Meteorol. Climatol. 51, 829–841. https://doi.org/10.1175/JAMC-D-11-0180.1.
Perret, L., Savory, E., 2013. Large-scale structures over a single street canyon immersed in an urban-type boundary layer. Boundary-Layer Meteorol. 148, 111–131. https://doi.org/10.1007/s10546-013-9808-z.
Ramponi, R., Blocken, B., 2012. CFD simulation of cross-ventilation for a generic isolated building: impact of computational parameters. Build. Environ. 53, 34–48. https://doi.org/10.1016/j.buildenv.2012.01.004.
Ricci, A., Burlando, M., Repetto, M.P., Blocken, B., 2019. Simulation of urban boundary and canopy layer flows in port areas induced by different marine boundary layer inflow conditions. Sci. Total Environ. 670, 876–892. https://doi.org/10.1016/j.scitotenv.2019.03.230.
Richards, P.J., Hoxey, R.P., 1993. Appropriate boundary conditions for computational wind engineering models using the k-ε turbulence model. J. Wind Eng. Ind. Aerod. 145–153. https://doi.org/10.1016/B978-0-444-81688-7.50018-8.
Salim, S.M., Buccolieri, R., Chan, A., Sabatino, S. Di, 2011a. Numerical simulation of atmospheric pollutant dispersion in an urban street canyon: comparison between RANS and LES. Jnl. Wind Eng. Ind. Aerodyn. 99, 103–113. https://doi.org/10.1016/j.jweia.2010.12.002.
Salim, S.M., Cheah, S.C., Chan, A., 2011b. Numerical simulation of dispersion in urban street canyons with avenue-like tree plantings: comparison between RANS and LES. Build. Environ. 46, 1735–1746. https://doi.org/10.1016/j.buildenv.2011.01.032032.
Scungio, M., Stabile, L., Rizza, V., Pacitto, A., Russi, A., Buonanno, G., 2018. Lung cancer risk assessment due to traffic-generated particles exposure in urban street canyons: a numerical modelling approach. Sci. Total Environ. 631–632, 1109–1116. https://doi.org/10.1016/j.scitotenv.2018.03.093.
Sergent, E., 2002. Vers une méthodologie de couplage entre la simulation des grandes échelles et les modèles statistiques. Ecully, Ecole centrale de Lyon.
Stabile, L., Arpino, F., Buonanno, G., Russi, A., Frattolillo, A., 2015. A simplified benchmark of ultrafine particle dispersion in idealized urban street canyons: a wind tunnel study. Build. Environ. 93, 186–198. https://doi.org/10.1016/j.buildenv.2015.05.045.
Stathopoulos, T., Zhu, X., 1988. Wind pressures on building with appurtenances. J. Wind Eng. Ind. Aerod. 31, 265–281. https://doi.org/10.1016/0167-6105(88)90008-6.
Tominaga, Y., Mochida, A., Yoshie, R., Kataoka, H., Nozu, T., Yoshikawa, M., Shirasawa, T., 2008. AIJ guidelines for practical applications of CFD to pedestrian wind environment around buildings. J. Wind Eng. Ind. Aerod. 96, 1749–1761. https://doi.org/10.1016/j.jweia.2008.02.058.
Tominaga, Y., Stathopoulos, T., 2013. CFD simulation of near-field pollutant dispersion in the urban environment: a review of current modeling techniques. Atmos. Environ. 79, 716–730. https://doi.org/10.1016/j.atmosenv.2013.07.028.
Tominaga, Y., Stathopoulos, T., 2011. CFD modeling of pollution dispersion in a street canyon: comparison between LES and RANS. J. Wind Eng. Ind. Aerod. 99, 340–348. https://doi.org/10.1016/j.jweia.2010.12.005.
Tominaga, Y., Stathopoulos, T., 2007. Turbulent Schmidt numbers for CFD analysis with various types of flowfield. Atmos. Environ. 41, 8091–8099. https://doi.org/10.1016/j.atmosenv.2007.06.054.
Vasaturo, R., Kalkman, I., Blocken, B., Wesemael, P.J.V. Van, 2018. Large eddy simulation of the neutral atmospheric boundary layer: performance evaluation of three inflow methods for terrains with different roughness. J. Wind Eng. Ind. Aerod. 173, 241–261. https://doi.org/10.1016/j.jweia.2017.11.025.
Vervoort, R., Blocken, B., van Hooff, T., 2019. Reduction of particulate matter concentrations by local removal in a building courtyard: case study for the Delhi

American Embassy School. Sci. Total Environ. 686, 657–680. https://doi.org/10.1016/j.scitotenv.2019.05.154.
Vranckx, S., Vos, P., Maiheu, B., Janssen, S., 2015. Impact of trees on pollutant dispersion in street canyons: a numerical study of the annual average effects in Antwerp, Belgium. Sci. Total Environ. 532, 474–483. https://doi.org/10.1016/j.scitotenv.2015.06.032.
Walton, A., Cheng, A.Y.S., 2002. Large-eddy simulation of pollution dispersion in an urban street canyon—Part II: idealised canyon simulation. Atmos. Environ. 36, 3615–3627. https://doi.org/10.1016/S1352-2310(02)00260-1.
Wang, C., Li, Q., Wang, Z.-H., 2018. Quantifying the impact of urban trees on passive pollutant dispersion using a coupled large-eddy simulation – Lagrangian stochastic model. Build. Environ. 145, 33–49. https://doi.org/10.1016/j.buildenv.2018.09.014.
Wen, H., Malki-Epshtein, L., 2018. A parametric study of the effect of roof height and morphology on air pollution dispersion in street canyons. J. Wind Eng. Ind. Aerod. 175, 328–341. https://doi.org/10.1016/j.jweia.2018.02.006.
Werner, H., Wengle, H., 1993. Large-eddy simulation of turbulent flow over and around a cube in a plate channel. In: Turbulent Shear Flows 8. Springer Berlin Heidelberg, Berlin, Heidelberg, pp. 155–168. https://doi.org/10.1007/978-3-642-77674-8_12.
World Health Organization, 2016. WHO Global Urban Ambient Air Pollution Database (Update 2016). Geneva, Switzerland.
Xie, X., Hao, C., Huang, Y., Huang, Z., 2020. Influence of TiO2-based photocatalytic coating road on traffic-related NOx pollutants in urban street canyon by CFD modeling. Sci. Total Environ. 724, 138059. https://doi.org/10.1016/j.scitotenv.2020.138059.
Zhang, K., Chen, G., Wang, X., Liu, S., Mak, C.M., Fan, Y., Hang, J., 2019. Numerical evaluations of urban design technique to reduce vehicular personal intake fraction in deep street canyons. Sci. Total Environ. 653, 968–994. https://doi.org/10.1016/j.scitotenv.2018.10.333.
Zhang, Y.-W., Gu, Z.-L., Cheng, Y., Lee, S.-C., 2011. Effect of real-time boundary wind conditions on the air flow and pollutant dispersion in an urban street canyon—large eddy simulations. Atmos. Environ. 45, 3352–3359. https://doi.org/10.1016/j.atmosenv.2011.03.055.
Zheng, X., Montazeri, H., Blocken, B., 2020. CFD simulations of wind flow and mean surface pressure for buildings with balconies: comparison of RANS and LES. Build. Environ. 173, 106747. https://doi.org/10.1016/j.buildenv.2020.106747.
Zhong, J., Cai, X.-M., Bloss, W.J., 2017. Large eddy simulation of reactive pollutants in a deep urban street canyon: coupling dynamics with O3-NOx-VOC chemistry. Environ. Pollut. 224, 171–184. https://doi.org/10.1016/j.envpol.2017.01.076.
Zhong, J., Cai, X.-M., Bloss, W.J., 2015. Modelling the dispersion and transport of reactive pollutants in a deep urban street canyon: using large-eddy simulation. Environ. Pollut. 200, 42–52. https://doi.org/10.1016/j.envpol.2015.02.009.